THESIS FOR THE DEGREE OF LICENTIATE OF ENGINEERING

ELECTRON BEAM MELTING OF ALLOY 718

POWDER RECYCLING AND ITS EFFECT ON DEFECT FORMATION

Hans Gruber

Department of Industrial and Materials Science

CHALMERS UNIVERSITY OF TECHNOLOGY

Gothenburg, Sweden 2019

Electron Beam Melting of Alloy 718
Powder Recycling and its Effect on Defect Formation
Hans Gruber

Technical report no. IMS-2019-1

Department of Industrial and Materials Science
Chalmers University of Technology
SE-412 96 Gothenburg
Sweden
Telephone + 46 (0)31-772 1000

Printed by Chalmers digitaltryck
Gothenburg, Sweden 2019

Electron Beam Melting of Alloy 718

POWDER RECYCLING AND ITS EFFECT ON DEFECT FORMATION

Hans Gruber

Department of Industrial and Materials Science

Chalmers University of Technology

Abstract

As for any production process, the performance of additively manufactured components is ultimately dependent on the quality of the feedstock material. Consequently, for critical components, the feedstock needs to be carefully controlled to assure a stable and reliable quality. At the same time, the materials efficiency of additive manufacturing is closely related to powder recycling, which may affect both physical and chemical properties of the powder. This is especially the case for electron beam melting (EBM) where the recycled powder may change significantly from exposure at the high temperature in the build chamber.

The aim of this study is to investigate the connection between powder recycling, powder chemistry and presence of defects in EBM processed Alloy 718. For this purpose, recycled powder was studied with reference to its virgin counterpart to detect differences in surface morphology, surface chemical composition as well as bulk chemistry as a consequence of powder recycling. The amount of defects and their distribution in samples produced from virgin and recycled powder was studied by means of image analysis and oxygen measurements. Morphological analysis using scanning electron microscopy was performed to understand their origin and formation mechanism.

The results show a significant change in surface characteristics after exposing the powder to the process and the environment in the build chamber. While the virgin powder is covered by a relatively thin and homogeneous oxide layer, the recycled powder has undergone transformation to a heterogeneous oxide layer rich in thermodynamically stable Al-rich oxide particulates. Significant growth of the Al-rich oxide occurs via selective oxidation of Al at the conditions in the build chamber, including both pick-up of oxygen from the process atmosphere and re-distribution of oxygen from less stable oxide products. The increasing amount of oxide is confirmed by an increase in total oxygen level with progressive recycling.

Furthermore, a clear correlation between the powder oxygen level and the amount of oxide inclusions in the EBM fabricated samples was observed. Hot isostatic pressing can be used to reach a near-full densify in samples produced from virgin powder. The samples produced from recycled powder, however, have a higher amount of aluminium-rich oxide inclusions which remain after HIP treatment. A variety of oxide defects was observed, ranging from finely dispersed oxide particulates inside lack of fusion defects to large oxide agglomerates in the bulk metal. Based on their morphology, it is shown that most of them originate from aluminium-rich oxide particulates on the surface of the recycled powder. It is suggested that the quality of EBM processed Alloy 718 is at present dependent on the oxygen level in the powder in general and the surface chemistry of the powder in particular, which needs to be controlled to maintain a low amount of inclusion defects.

Preface

This licentiate thesis is based on the work performed at the Department of Industrial and Materials Science at Chalmers University of Technology, Gothenburg, Sweden between June 2016 and December 2018. The project has been carried out under supervision of Professor Eduard Hryha and Professor Lars Nyborg.

List of appended papers

I. **Effect of Recycling Alloy 718 Powder in Electron Beam Melting**
H. Gruber, M. Henriksson, H. Hryha, L. Nyborg
Submitted for journal publication

II. **Effect of Powder Recycling on the Fracture Behaviour of Electron Beam Melted Alloy 718**
H. Gruber, P. Karimi, H. Hryha, L. Nyborg
Powder Metallurgy Progress, Vol. 18, 2018

III. **Effect of Powder Recycling on Defect Formation in EBM Processed Alloy 718**
H. Gruber, C. Luchian, H. Hryha, L. Nyborg
Submitted for journal publication

Contribution to the appended papers

I. The author planned and executed the majority of the experimental work and the analysis of the results. The author assisted in the AES analysis. The author wrote the paper in cooperation with the co-authors.

II. The author planned and executed the majority of the experimental work and the analysis of the results. The author wrote the paper in cooperation with the co-authors.

III. The author planned and executed the majority of the experimental work and the analysis of the results. The author wrote the paper in cooperation with the co-authors.

Contents

1. Introduction 1

1.1 Aims and objectives 2

2. Superalloys 3

1.1 Alloy 718 3

3. Metal additive manufacturing 4

3.1 Powder bed fusion 4

3.1.1 The PBF build cycle 4

3.1.2 The scanning strategy 4

3.1.3 Powder for PBF 5

3.1.4 The process environment 6

3.2 Powder recycling 7

3.2.1 High temperature oxidation 9

3.2.2 Powder oxidation 10

4. Defects in additive manufactured superalloys 15

4.1 Defects in EBM processed Alloy 718 16

4.1.1 Non-metallic inclusions 16

4.1.2 Lack of fusion defects 23

5. Experimental procedure 25

5.1 Material 25

5.2 Analysis techniques 26

6. Summary of results in appended papers 29

7. Conclusions 35

Future work 37

Acknowledgements 39

References 41

1. INTRODUCTION

Additive manufacturing (AM) offers great opportunities in product development and production in many aspects. Commonly mentioned benefits are reduced lead times, reduced material consumption, increased design freedom and part consolidation, to name a few. Within AM, electron beam melting (EBM) is a powder bed fusion (PBF) process in which a high power electron beam is used to build the parts by selective melting of thin layers in a metal powder bed, according to the geometry from a CAD-file. Among other applications, EBM is seen as a potential method for near-net-shape production of aerospace and power generation components, which are often made from materials, which are both difficult and inefficient to process using traditional manufacturing methods, as in the case of Ni- and Ni-Fe-base superalloys.

Superalloys are often used in critical safety applications such as rotating parts in aerospace engines. In such cases, careful control of both raw material and process is required to reach an adequate quality assurance. In particular, the performance of such components is largely dependent on keeping a low amount of non-metallic inclusions (NMIs) [1], such as oxide and nitride inclusions. For example, presence of NMIs is known to be a common reason for fatigue failure, which in turn is a common cause for failure in rotating parts in aerospace engines [2].

NMIs form during the melting process due to the presence of oxygen and nitrogen in the raw material or in the processing atmosphere. Furthermore, due to the high thermal and chemical stability of NMIs, very little modification is possible through heat treatment post-processing. Therefore, in traditional superalloy metallurgy, presence of large NMIs in critical parts has been limited by careful selection of the raw material and by applying a series of vacuum melting and refining steps where the impurity level is reduced to acceptable levels.

Compared to other processes, the small volume of material in liquid state and the high solidification rate in AM limits the size of NMIs that can form. Therefore, in this sense, AM is a potential candidate for production of clean materials [3]. However, as known from traditional powder metallurgy, the metal powder used for AM is sensitive to surface oxidation. This is especially critical for superalloys powder which often contain reactive elements. At first hand, this sets high requirements on the actual powder production to reach sufficiently low oxygen levels. In addition, oxidation of the powder may occur as a consequence of handling/storage and due to exposure in the AM machine process environment. The latter is the most critical factor in this respect since the high materials efficiency in PBF relies on powder recycling, i.e. re-use of the non-consumed powder in subsequent build cycles. The extent to which powder recycling can be permitted before risking loss in part performance is therefore a key issue for PBF as a viable manufacturing process.

It is known that powder recycling in AM, in general, has an influence on both physical and chemical powder properties [4]. Regarding powder oxidation, electron beam melting is especially critical due to the high temperature in the build chamber. However, the resulting effects of powder recycling on the part quality is generally quite unexplored. This is especially the case for EBM processed Alloy 718 where published results are almost non-existing.

1.1 Aims and objectives

The aim of this research is to provide basic understanding regarding recycling of Alloy 718 powder during EBM processing and its effect on the quality of built components. From this topic, three main research questions have been formulated:

- What is the effect of powder recycling on the surface chemistry of Alloy 718 powder?
- What is the effect of powder recycling on the amount and distribution of defects in EBM processed Alloy 718?
- What is the effect of powder recycling on the fracture behaviour of EBM processed Alloy 718?

Particular interest lies in the surface oxidation of the powder at the high temperature conditions in the EBM process chamber as this may considerably change the performance of the powder in its role as feedstock material for production of AM components. Furthermore, a quantitative correlation between powder recycling, in terms of oxygen pick-up during EBM processing, and the quality of EBM processed samples is sought. The latter is evaluated in terms of the amount and distribution of defects in samples built from virgin and re-used powder, respectively. Finally, the defect population in samples built from progressively re-used powder is carefully characterized to determine their formation mechanisms as well as their influence on mechanical performance.

2. SUPERALLOYS

Superalloys is a group of materials developed for elevated temperature service where an adverse set of high mechanical, thermal and chemical loads may be encountered. Superalloys retain their properties to higher homologous temperatures than any other widely used commercial alloy system [2]. Therefore, they are the typical materials to be employed in high temperature engineering components, such as in the hot sections of aircraft jet engines and other gas turbines. However, due to their excellent properties, superalloys also see service in a wide range of other industrial application areas such as rocket motors, power plants, automotive engines, hot work tools and dies as well as in the chemical industry. Based on their major alloying elements, superalloys are commonly divided into nickel-, cobalt-, iron-, and nickel-iron-base superalloys [2].

1.1 Alloy 718

Alloy 718 (also known as Inconel® 718 or IN718) is a well-known precipitation strengthened Ni-Fe-base superalloy. Since the development of the alloy in the late 1950's, it has been the workhorse for hot structural turbine engine components at working temperatures up to around 650°C [5, 6]. It is known to be the material of choice for many gas turbine disc and rear frame applications, but has also earned success in the automotive, nuclear, oil and gas industries [2]. It is still the predominant superalloy in the world and constitutes one-third of the total weight of some aero engines [6].

The chemical composition of Alloy 718 is listed in Table 1. In contrast to many other superalloys, Alloy 718 is developed to maximize strength at low to intermediate temperature [2]. This is achieved by additions of Nb which promotes precipitation of the intermetallic phase γ" (Ni_3Nb). The γ" phase develops effective coherency strains relative to the matrix from which Alloy 718 owns the main part of its high strength [2]. However, this also limits its strength to temperatures of around 650°C, above which a rapid loss in strength may occur due to particle coarsening [2]. This is also the lower temperature for formation of the δ phase which is the thermodynamically stable form of γ". Furthermore, the sluggishness of the γ" precipitation gives the Alloy 718 a high resistance to strain age cracking which is a problem for many superalloys [2].

Due to small additions of Al and Ti (0.5 and 1.0 wt.%, respectively), a smaller amount of the matrix-coherent γ' ($Ni_3(Al, Ti)$) also contributes to the precipitation strengthening. However, the amount of γ' is only around 5 vol.%, which is much lower compared to that of many other superalloys [5]. A few percent of Al is also added in many Ni-base superalloys to enhance the oxidation resistance. In Alloy 718, however, the corrosion and oxidation resistance relies on the addition of Cr. The relatively high Fe content gives it a competitive price and improved forgeability [5, 7]. Apart from the elements listed in Table 1, careful control must be taken to limit the amount of so called tramp elements such as O, N, S, P, Pb and Cu, which may have a detrimental influence on alloy performance. The phases present in Alloy 718 and their role in Alloy 718 can be found in [5].

Table 1. Alloy 718 chemical composition in wt.% according to AMS 5662 [8]

Element	*Ni*	*Cr*	*Fe*	*Nb*	*Mo*	*Ti*	*Al*	*C*	*Ta*	*Co*	*Mn*	*B*	*Si*
Min	*50.0*	17.0	Bal.	4.75	2.8	0.65	0.2	-	-	-	-	-	-
Max	*55.0*	21.0	Bal.	5.5	3.3	1.15	0.8	0.08	0.05	1.0	0.35	0.006	0.35

3. METAL ADDITIVE MANUFACTURING

Additive manufacturing (AM), also known as 3D printing, is a family of manufacturing technologies in which parts are fabricated by adding material in thin successive 2D slices, derived from the geometry of a CAD model [9]. AM involves several different techniques for various materials and applications, among which the two largest for fabrication of metal components are powder bed fusion (PBF) and direct energy deposition (DED). Among these two, PBF generally possesses a higher geometrical accuracy (enables melting of overhangs), while DED is typically associated with higher deposition rates [10].

PBF offers near-net-shape production of geometrically complex parts without the need for moulds and tooling. This offers a reduction in cost, lead time and resources compared to many other metal working processes [4, 11, 12]. Its high degree of design freedom makes it well suited for smaller production series of high-value, complex shaped components where lightweight or integrated functionality is desired [13]. This has been identified by different industries, including the aerospace sector, especially for processing of expensive materials with poor fabricability. This is generally the case for Ni-base and Ni-Fe-base superalloys [3, 11, 12, 14, 15], which, due to their high strength at elevated temperature, are known as some of the most "difficult-to-machine materials" [16]. In addition, high material costs and increasing demands on sustainable production routes further incentivize minimum machining and improved buy-to-fly ratio [17, 18].

3.1 Powder bed fusion

In PBF, the parts are built by means of successive melting of layers in a metal powder bed using a focused energy source [4, 7]. The PBF is commonly further divided into two subgroups, namely laser powder bed fusion (LPBF) and electron beam melting (EBM®) [4]. As implied by their names, one important difference between these two techniques is that they use different thermal sources for melting the powder - a laser beam in LPBF and an electron beam in EBM. As will be described later on, this implies some further characteristic differences between them. However, the basic working principle, as illustrated in Fig. 1, using the EBM machine interior, remains similar.

3.1.1 The PBF build cycle

Generally, the PBF build cycle starts with distribution of powder in a thin layer across a start plate onto which the parts are built. The powder layer is selectively melted according to the build geometry in the current layer. The build platform is then lowered by a distance equal to one layer thickness (between 20-50 μm for LPBF and 50-100 μm for EBM) and a new layer is spread and melted on top of the previous. Re-melting of the adjacent layers is done to avoid bonding defects between the layers. This sequence is repeated until the parts have been successfully built. When the build cycle is completed, the non-consumed powder, which can constitute a large portion of the build tank, is evacuated from the chamber. Separating the parts from the start plate is done in a separate process.

3.1.2 The scanning strategy

During melting, the beam moves according to a pre-defined scan pattern. Together with the process parameters (beam power, scan speed, layer thickness, etc.), the scan pattern forms the so called scanning strategy, which has a strong influence on several important features such as porosity, microstructure, surface roughness and residual stresses [4]. Consequently, different scan strategies have been found suitable for different technique/material combinations.

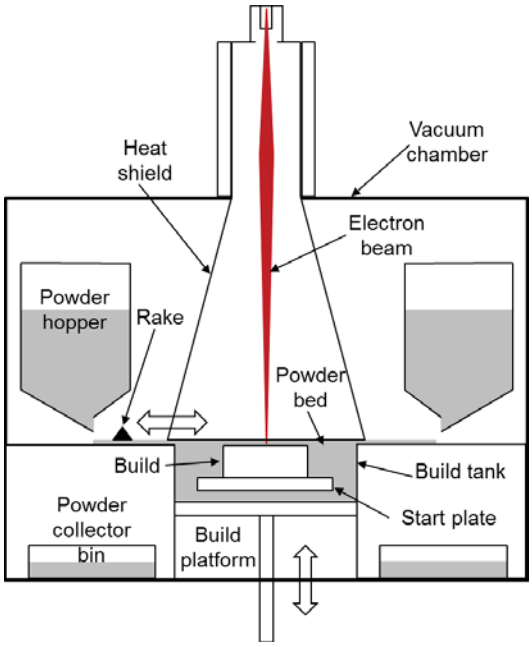

Fig. 1. Schematic of the EBM machine interior. Grey areas constitute metal powder. Redrawn from [19].

In EBM, the scan strategy has been chosen as to improve the surface finish by lowering the part temperature when creating its surface. This is done by applying one or several high energy spot melting passes (called multi-spot) at the edges (commonly referred to as the contour region) before scanning of the part core, see. Fig. 2 [7]. The EBM core pattern, usually referred to as the hatch pattern, is usually uni-directional or bi-directional, see Fig. 2, and is rotated for a certain angle between each layer [7]. Overlapping between the hatch and contour is done to improve the density at the interface. In LPBF, where the build temperature is lower, the scan pattern at the edges is usually continuous and is done after the hatch exposure [7].

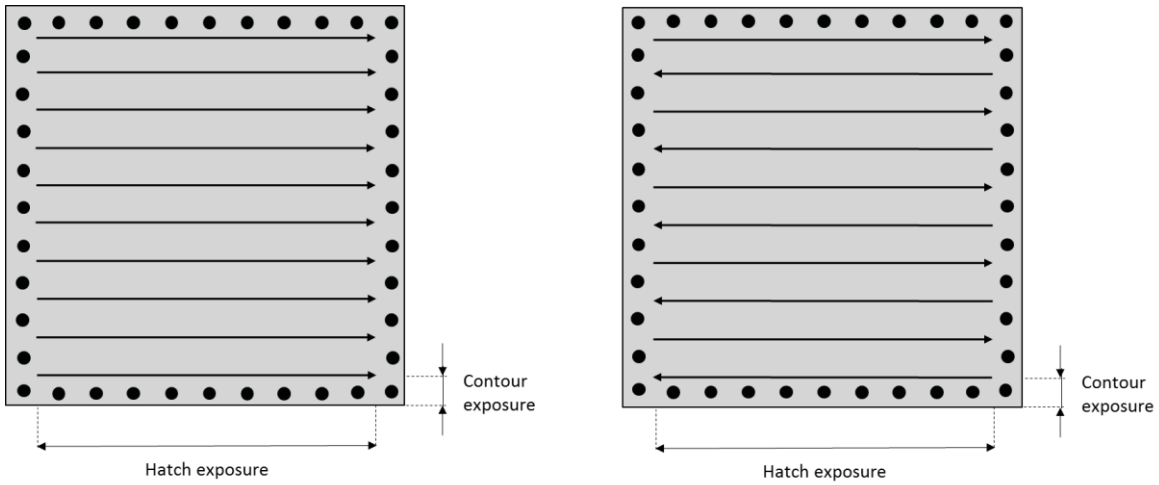

Fig. 2. Uni-directional and bi-directional scanning patterns in EBM. Redrawn from [19].

3.1.3 Powder for PBF

The most common fabrication method for commercial pre-alloyed powders for PBF is gas atomization (GA), in which the powder is atomized in a stream of inert gas. In inert gas atomization, the raw material is melted in an inert gas atmosphere. It is mostly used for production of less reactive materials such as aluminium and different types of steels [20]. For materials which

are alloyed with reactive elements (such as Al and Ti in many Ni-base superalloys), reactions with oxygen and nitrogen during atomization is limited by melting the raw material in a controlled vacuum atmosphere prior to the atomization such as in the vacuum induction gas atomization (VIGA). According to specifications from powder producers [21], the oxygen and nitrogen levels in VIGA produced superalloy powder are commonly below 300 ppm. One major source of contamination and the limitation for cleanliness and performance of this kind of powder is interaction with the refractory system that is in contact with the melt during melting and molten metal transfer [2]. This has led to development of the so called ceramic-less powder atomizing techniques where the powder is produced by direct atomization of a wire or rod precursor material, such that the molten metal does not come into contact with refractories [2]. Some examples are electrode induction gas atomization (EIGA), plasma rotating electrode process (PREP) as well as plasma atomization (PA, also referred to as advanced plasma atomization, APA™, developed by AP&C, Canada, which is a subsidiary of GE Additive). In PA, a high velocity argon plasma is used to atomize the wire precursor material at a very high temperature. The PA enables production of highly spherical powder (see Fig. 3) with higher purity than the gas atomized powder [22]. It should be noted, however, that the purity of EIGA and PA manufactured powder grades is largely dependent on the quality of the precursor material.

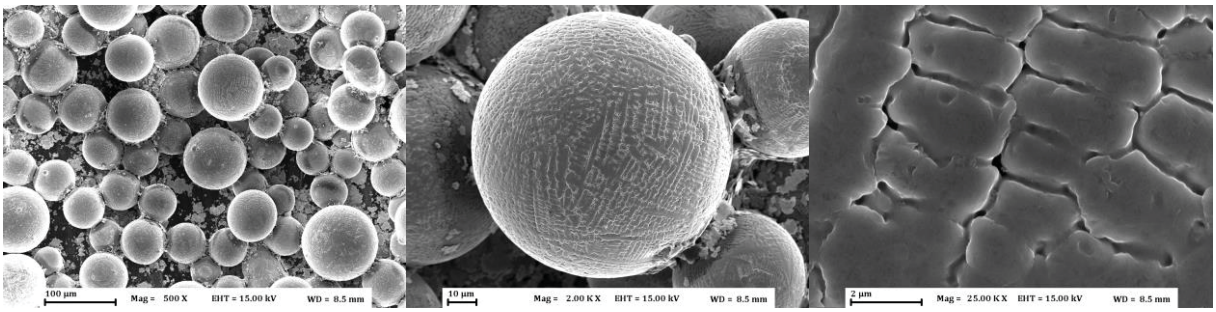

Fig. 3. AP&C's Alloy 718 powder produced by advanced plasma atomization. Author's experimental result.

3.1.4 The process environment

As already mentioned, the difference in energy source implies some other characteristic differences between LPBF and EBM. Both processes take place in protective atmospheres to prevent the hot metal surfaces from oxidation or other interactions with reactive atmospheric gases. The atmosphere in the LPBF is usually obtained by purging the process chamber with an inert gas (such as argon or nitrogen) to an oxygen concentration of around 1000 ppm [23]. The EBM process, on the other hand, requires a low vacuum to prevent collision of the electrons with gas molecules, which would deflect the beam and thereby lower its efficiency [7, 24]. The vacuum in the EBM chamber is created by first lowering the pressure inside the process chamber to below 1 x 10^{-8} bar. From an oxidation point of view, the vacuum should be as low as possible since the oxygen level stands in direct relation to the total pressure in the chamber. However, the system size and complexity as well as the sublimation of volatile alloying elements set practical limits to the achievable vacuum level. Sublimation is reduced by creating a partial pressure of inert gas during the process [2]. This is done by injecting a small amount of grade 5 purity helium (<2 ppm O_2), which raises the pressure in the build chamber to around 2 x 10^{-6} bar. From this, a theoretical oxygen partial pressure of around 4x10^{-9} bar inside the build chamber has be estimated [19]. The pressure, but not the oxygen level, is continuously measured and logged.

Another important characteristic of the EBM process is the fact that the powder bed is held at an elevated temperature throughout the whole build process. One reason for this is that the powder

bed needs to have a sufficient conductivity and mechanical stability to avoid so called powder smoking. This originates in the electrical negative charge induced to the metal particles from the incoming electrons in the electron beam which may result in repulsion of the powder if the electrical forces become larger than those holding them in place [9]. Therefore, after the spreading of each powder layer, it is heated with the electron beam to create slight bonding between the metal particles [5, 11]. The elevated temperature also increases the stability of the melting process and varies between 600-1100°C depending on the processed material. For Alloy 718, a temperature of 975±25°C has been noted as optimal to reach a stable process [7, 19]. Below 950°C, increased powder smoking and spatter from the melt pool has been observed [7].

Powder smoking is further prevented by the presence of helium in the build chamber, since He tends to dissipate electrical charge build-up on the powder when ionized by the electron beam [7]. Furthermore, the addition of He can also be used for faster cooling of the build volume after completing the build.

The temperature in the EBM process chamber is maintained by using a rapidly scanned, diffuse electron beam. The temperature is first established by heating the start plate and the powder around it, before spreading the first powder layer. A thermocouple attached under the start plate registers when the temperature is reached. Thereafter, in each layer iteration, the area over the start plate is heated, both before and after melting. The start plate temperature is logged throughout the whole process but cannot be used for feedback to control the temperature in the build volume and the energy input. Instead, a complex energy balance function that calculates the current and speed of the electron beam, based on the build geometry, is used to maintain the desired temperature [7].

Due to the high temperature in the build volume, parts fabricated by EBM have substantially lower residual stresses compared to LPBF, where the temperature in the build envelope is generally much lower [4]. Therefore, the EBM build plate can be held in place simply by sintering the powder that surrounds it (see Fig. 1). In LPBF, thick plates that are screwed to the machine feeding mechanism is required to avoid plate warping due to the high residual stresses that occur in the parts. This also makes EBM more suitable for processing of materials which are prone to cracking, such as precipitation hardened superalloys and intermetallics such as TiAl [11, 24]. Furthermore, unlike LPBF, the sintered powder bed in EBM acts as a natural support for the parts which can be stacked on top of each other in the build volume.

The risk of powder smoking in EBM can be further reduced by using a coarser powder (50-106 μm compared to 10-60 μm for LPBF) and a less focused electron beam. This results in thicker layers and larger melt pools, respectively, which in turn increases the productivity. However, this negatively affects the surface roughness and the geometrical precision which is generally better for LPBF [4, 9]. The productivity can be further increased since the electron beam is operated by electromagnetic lenses which allows for higher scan speeds compared to that in LPBF, for which mechanically moved mirrors are used for movement of the laser beam [4, 7, 9].

3.2 Powder recycling

Even though additive manufacturing has been subjected to extensive research during the last years, there is still lack in knowledge in many different aspects. One such area is the effect of the powder feedstock material on the process stability and/or quality of fabricated parts [25]. While several

physical and chemical powder characteristics have been suggested as being critical for maintaining a reliable process [26, 27], too few indications regarding the importance of these characteristics have been established.

Another relatively un-explored branch within the additive manufacturing research area is the possible degradation of the powder as a consequence of recycling, i.e. re-use of the non-consumed powder in subsequent build cycles. In the case of powder bed fusion, the non-consumed powder can constitute a large portion of the build volume after each completed build cycle. Powder recycling in additive manufacturing is crucial to reach a high materials efficiency and is therefore a key issue for PBF as a viable manufacturing process. This is essential both from a resource and an economical perspective, especially since powder is generally more expensive than more commonly used material feedstock, such as plate, bar or tubing.

The non-consumed powder is recycled according to a procedure specified by the machine producer. In LPBF, recycling involves sieving of the powder left in the build tank and the collector bins (see Fig.1), to remove any agglomerates that may appear after the process. The sieved powder is then mixed with the non-consumed powder from the powder hoppers before it is filled back into the machine. In the EBM process, due to the powder sintering, the non-consumed powder in the build tank (especially in the volume above and beneath the start plate) is in the shape of a "cake" of sintered powder, see Fig. 4. Therefore, in addition to the recycling procedure in LPBF, separation of the sintered powder particles is done by grit blasting. As the temperature in the hoppers is lower than in the build chamber, this powder is less affected and can be sieved without grit blasting. To add up for the powder that was consumed in the previous cycle, the re-used powder is commonly mixed with a certain amount of fresh powder before it is filled back into the powder hoppers.

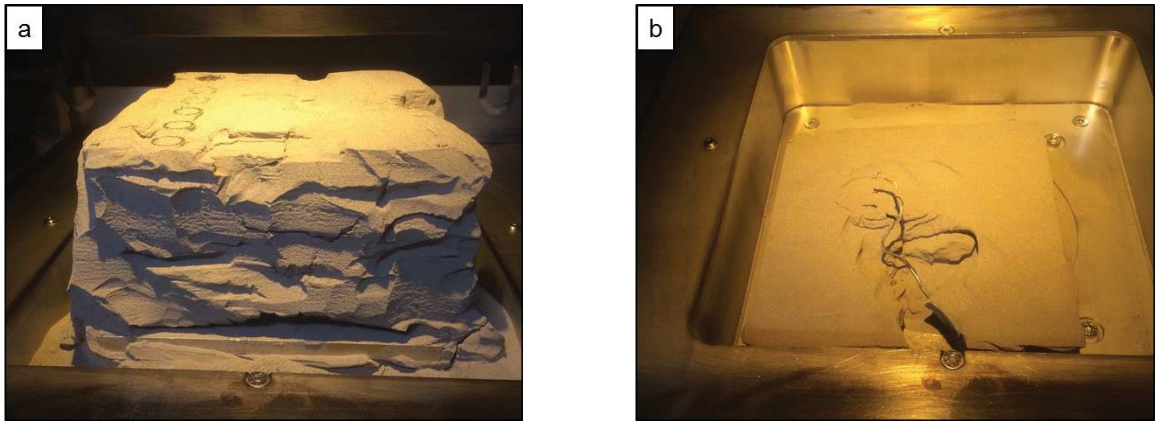

Fig. 4. Cake of sintered Alloy 718 powder (a) above and (b) below the start plate in an Arcam A2X EBM machine. Author's experimental result.

It is known that powder recycling in AM, in general, has an influence on both physical and chemical powder properties [4]. Regarding physical properties, it is known that for example powder size, shape and surface morphology often change during recycling. However, when it comes to resulting changes in part performance, no clear correlations have been established [4]. In terms of powder chemistry, increasing powder oxygen levels as a consequence of powder recycling have been noted for metal additive manufacturing in general [28-33]. Furthermore, it can be supposed that the high specific surface area of the AM powder makes it susceptible to surface reactions such as oxidation [34] and that the oxide on the powder surfaces may have a negative effect on wetting. As a

consequence, this may lead to increased porosity and reduced mechanical performance [28, 35]. Hence, powder oxidation has been suggested to be the limiting factor for powder re-use [29] and will therefore be treated more in detail in the following section. Oxidation, however, is a complex process, especially for highly alloyed superalloys. For this reason, some general aspects of oxidation are presented below, before powder oxidation is presented in section 3.2.2.

3.2.1 High temperature oxidation

The thermodynamic equilibrium conditions for a given metallic element and its oxide are defined by the oxygen partial pressure (pO_2) and the temperature. Figure 5 shows this relationship for the oxides that may occur in Alloy 718. At conditions above each curve, it is thermodynamically favourable for the element to exist in oxide state, while at conditions below the curve, it is more likely to find it in metallic state. As indicated in the figure, high temperature and/or low oxygen levels are required to prevent the metal from oxidation. Even though the data in Fig. 5 are based on oxidation of pure metals, it is still applicable for assessing the relative stability of oxides in an alloying system on a metal/gas surface. The dotted lines in Fig. 5 indicate the estimated conditions in the EBM process chamber, which will be discussed in section 3.2.2.

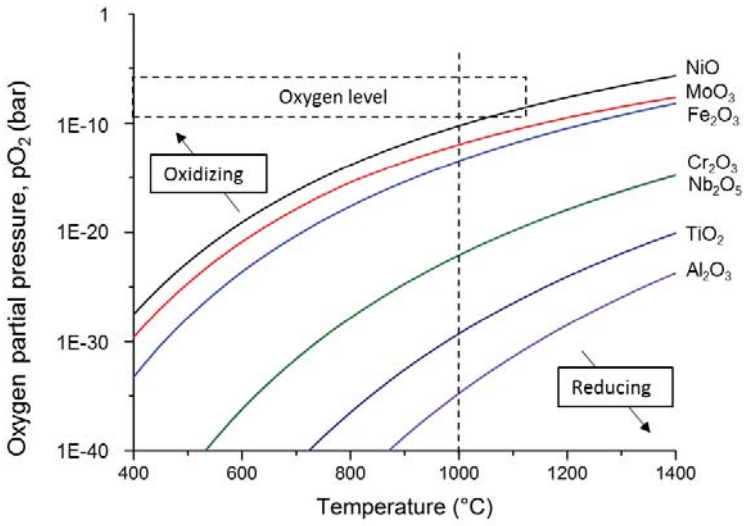

Fig. 5. Metal/metal oxide equilibria diagram. Plotted using data from the software HSC Chemistry version 8.0. Note the overlap of Cr_2O_3 and Nb_2O_5. The dotted lines indicate the estimated conditions in the EBM process chamber.

As can be seen in Fig. 5, there is a large difference in thermodynamic stability between the oxides. While nickel oxide is relatively unstable, some of the others, such as alumina and Ti-oxide, require very high temperature and/or low oxygen level for its reduction. From a thermodynamic point of view, due to their high affinity for oxygen, such elements are selectively oxidized compared to elements which form less stable oxides [2, 36].

Furthermore, both the extent of oxidation and the type of oxides found in the system depend on the kinetics, i.e. the mobility of elements through solid state diffusion. Even though aluminium forms the most stable oxide, its low bulk concentration in Alloy 718 (~0.5 wt. %) limits the amount that can react with oxygen at the surface. Instead, the vast amount of the bulk elements Ni, Cr and Fe render them as kinetically favourable oxide formers, among which Cr is the strongest oxide

former, see Fig.5. Therefore, a more or less continuous chromia scale is expected for Alloy 718 at the relatively low application temperature at which it is used [19, 37, 38].

However, as indicated above, the many alloying elements in superalloys make their oxidation behaviour rather complex and other oxide types such as multi- layered Ni-, Fe-rich oxides [38, 39] and spinel oxides are sometimes observed along with the chromia-scale [37, 40]. Furthermore, with increasing diffusion rates at higher temperature, both external and internal oxidation of minor reactive elements, such as Al and Ti, may occur [41, 42].

3.2.2 Powder oxidation

Powder compared to bulky materials are more prone to oxidation due to their high specific surface area which makes reactions with the atmosphere much more effective. In this case, the difference in oxygen potential between the surface and the bulk of the powder creates a strong driving force for mass transport of elements with high oxygen affinity towards powder surface. Furthermore, its small dimensions makes the maximum diffusion distance (which equals part of the powder radius) very short, which will further speed up reactions at elevated temperatures [34].

As the hot metal is exposed to oxygen during atomization, a certain amount of oxide on the powder surface is expected already in the as-atomized state. Figure 6 shows an example of two forms of surface oxide on the plasma atomized Alloy 718 powder used in this study. It partly consists of a bulk element oxide layer, which form at lower temperatures during production or subsequent handling, Fig. 6 (a). The limited diffusion at these temperatures typically results in thin homogeneous surface layers. Small amounts of strong oxide formers, such as Al and Ti, often results in heterogeneously distributed stable oxides, Fig. 6 (b), which may form at higher temperatures during the atomization process [43, 44].

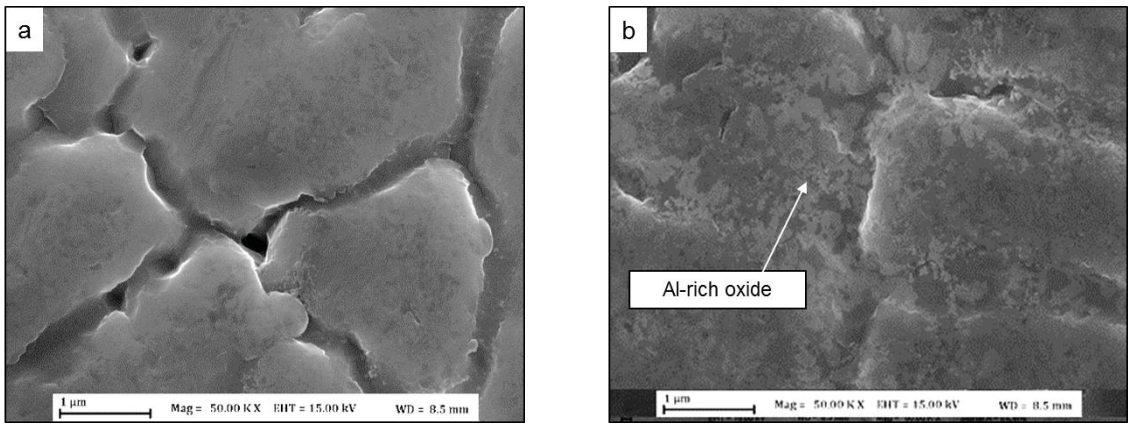

Fig. 6. Oxide products on virgin Alloy 718 powder produced by plasma atomization. Author's experimental result.

As a part of the manufacturing process, the powder can be passivated to create a thin, homogeneous passive layer which makes it more resistant to handling in open air [45]. Powder handling, including sieving (and grit blasting for EBM) in between the build cycles as well as during storage, when the powder is exposed to ambient air, may result in formation of hydroxides and/or uptake of chemisorbed and physisorbed water.

Powder oxidation in LPBF

In LPBF, the main part of the powder bed is too cold for significant oxidation to take place. Hence, oxidation of the non-consumed powder in LPBF is limited to the volume close to where melting

occurs (i.e. close to the fabricated parts) and to the so called process emissions or spatter that are emitted due to interaction between the powder and the laser beam. Among these emissions, the small sized condensate shows the highest extent of oxidation [45]. As an example, Fig. 7 shows differently affected Hastelloy X metal particles sampled at different positions in the process chamber, Fig. 7 (a).

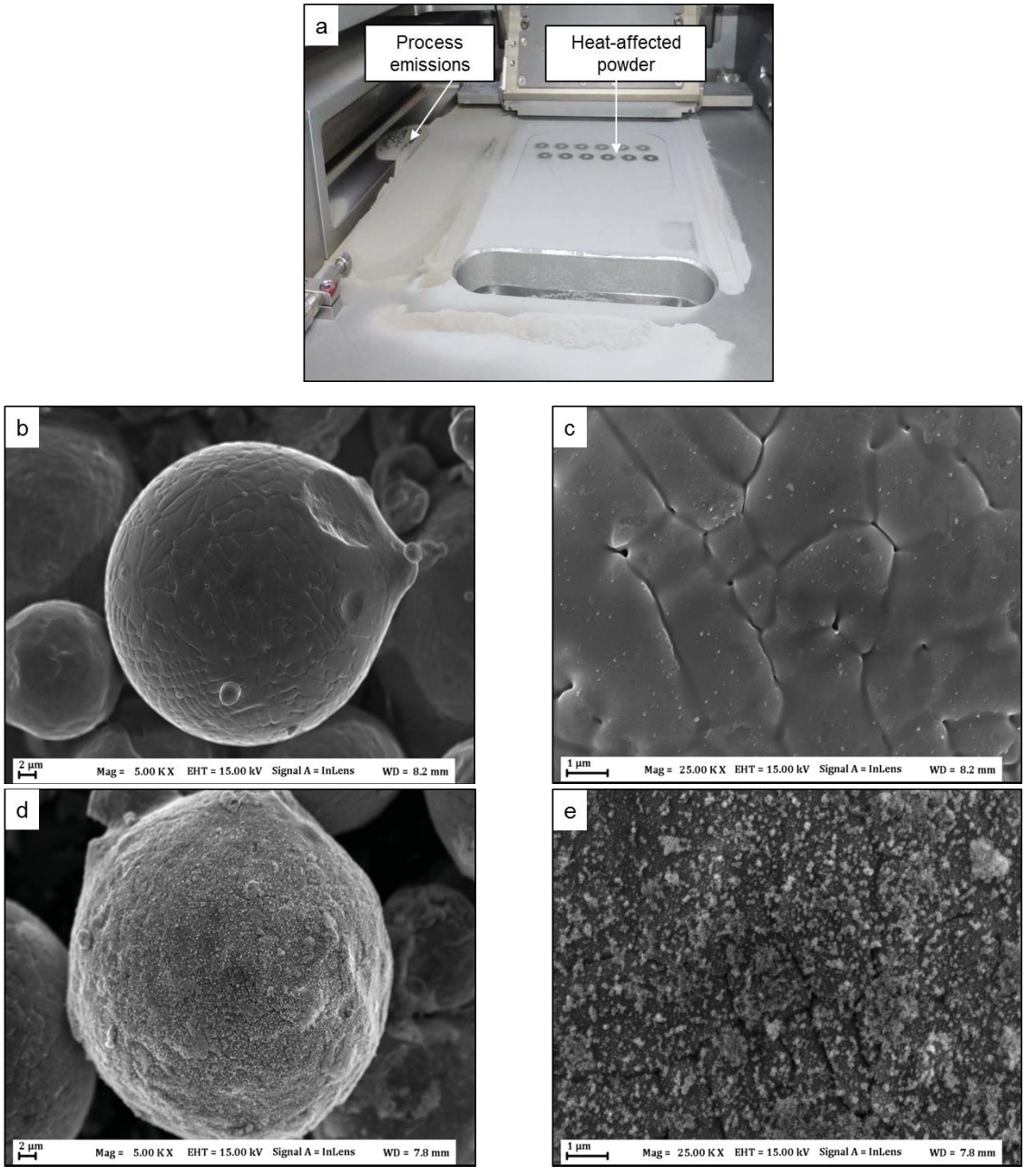

Fig. 7. a) LPBF process chamber with process emissions at the gas flow exhaust port (left side); b)-c) heat- affected particle sampled in between the parts in (a); d)-e) larger emission particle sampled at the gas flow exhaust port. Author's experimental result.

As seen in Fig. 7 (a), process emissions in LPBF follow the flow of the inert gas towards the exhaust port and will partly leave the chamber this way. Part of the emissions which do not reach the port will however end up in the powder bed, which will over time increase its overall oxygen level [45].

Figure 7 (b, c) shows a metal particle sampled from the volume close to the build parts, on which small oxide particulates have formed as a result of the increased temperature close to the molten metal. Figure 7 (d, e) shows an emitted Hastelloy X particle exhibiting significant oxidation (Cr-oxide), sampled from the gas flow exhaust port.

As mentioned above, significantly increased oxygen levels have in some cases been reported for recycled LPBF powder. Resulting effects on porosity and ductility have also been noted, but are usually reported to be quite limited [29, 46].

Powder oxidation in EBM

Also for EBM, increased oxygen levels have been measured for the recycled powder [25]. Though the resulting effect on the part performance has not been studied in detail, it is often stated that the excess powder can sustain a large number of cycles without any appreciable influence on its chemical properties [47] and that re-use of Alloy 718 powder during EBM processing is solely limited by the physical powder characteristics, such as flowability [25].

As the EBM process takes place under vacuum conditions, it is often marketed as a suitable alternative for processing of materials with high oxygen affinity [24]. Indeed, the oxygen level in the EBM build chamber is several orders of magnitude lower than in LPBF and therefore, oxidation of the actual melt pool material should be lower.

However, when it comes to powder recycling, the extent of powder oxidation in EBM differs from LPBF since the whole powder bed is held at a high temperature (~1000°C). This is known to be critical from the perspective of powder oxidation as the temperature is high enough for substantial diffusion to take place, and at the same time too low for efficient reduction of most oxides at practical pO_2 levels [34]. This is illustrated in the metal/metal oxide equilibria diagram in Fig. 5 where the estimated conditions in the EBM process chamber have been indicated. It can be seen that all of the potential oxides besides NiO and Fe_2O_3 are highly stable at these conditions. Hence, presence of one or several of these oxides is very likely at these conditions [48].

Powder bed fusion is associated with long process times where one single cycle can take several days. As the build volume often contains large amounts of non-consumed powder, it is very likely that a large portion of the powder may experience several re-use cycles. Therefore, it can be assumed that the accumulated exposure time at high temperature is more than enough for substantial oxidation to take place. The time and temperature required for a certain increase in oxygen level can be estimated using simple diffusion calculations.

Furthermore, prolonged high temperature exposure may result in re-distribution of oxygen between oxides with different stability when the conditions are reducing for less stable compounds and oxidizing with respect to the more stable ones [36]. Therefore, oxygen existing as bulk oxide/hydroxide formed during atomizing and/or powder handling (applies to virgin as well as re-used powder in between the build cycles), may be released during heating and melting of the powder in the process chamber. Consequently, as indicated in Fig. 5, the actual oxygen partial pressure in the vicinity of the powder surface can be higher than the theoretical and can locally rise to values in the order of 10^{-7} bar [19]. It should be noted however that these values are only valid assuming the system is air-tight since leakage of air into the chamber may dilute the He-containing atmosphere and thereby increase the oxygen concentration without necessarily changing the pressure.

In any case, instead of being evacuated from the process chamber, the released oxygen may act as additional source (in addition to the residual air in the vacuum atmosphere) which is consumed by strong oxide formers such as Al, present at the powder surface, for which these conditions are strongly oxidizing [36]. In such a case, transformation from less stable to more stable oxides results in an initial distribution of co-existing bulk element oxides and more stable oxides. Since the stable oxides will persist also at very high temperatures and/or low oxygen partial pressures, the amount of stable oxide on the powder surface will increase over the re-use cycles. This means that the chemistry and thereby the quality of the powder may be considerably changed. This situation is shown for Alloy 718 powder in Fig. 8, where the powder surface coverage of stable Al-rich oxide particulates increases with progressive re-use. With reference to the virgin powder in Fig. 3, it can be seen from Fig. 8 (a-c) that oxidation starts already during the first the first build cycle, after which it progresses with increasing powder re-use, see Fig. 8 (d-i).

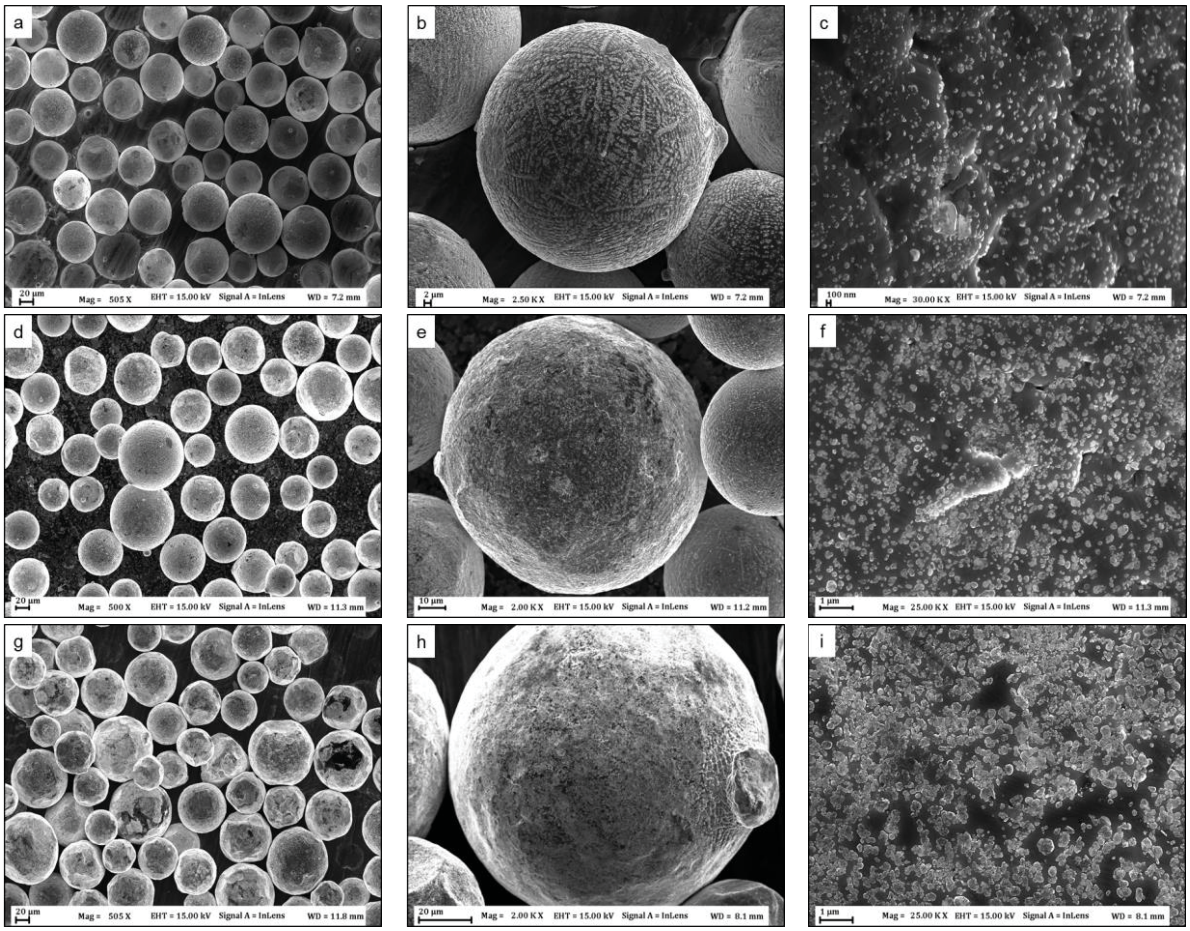

Fig. 8. Progressively re-used Alloy 718 EBM powder sampled from the cake of sintered powder after (a-c) 1 cycle; (d-f) 5 cycles (g-i) 30 cycles. Author's experimental result.

Furthermore, as shown in Fig. 9, owing to the long-term exposure at elevated temperature in the EBM process chamber, the powder microstructure changes from a dendritic solidification structure in the virgin powder, Fig. 9 (a), to a microcrystalline structure in the recycled condition, Fig. 9 (b). Furthermore, as evident from the EDS maps in Fig. 9 (c), the needle-shaped δ-phase (Ni_3Nb) forms as a consequence of the enhanced diffusion at the elevated temperatur and is therefore often present in the recycled powder.

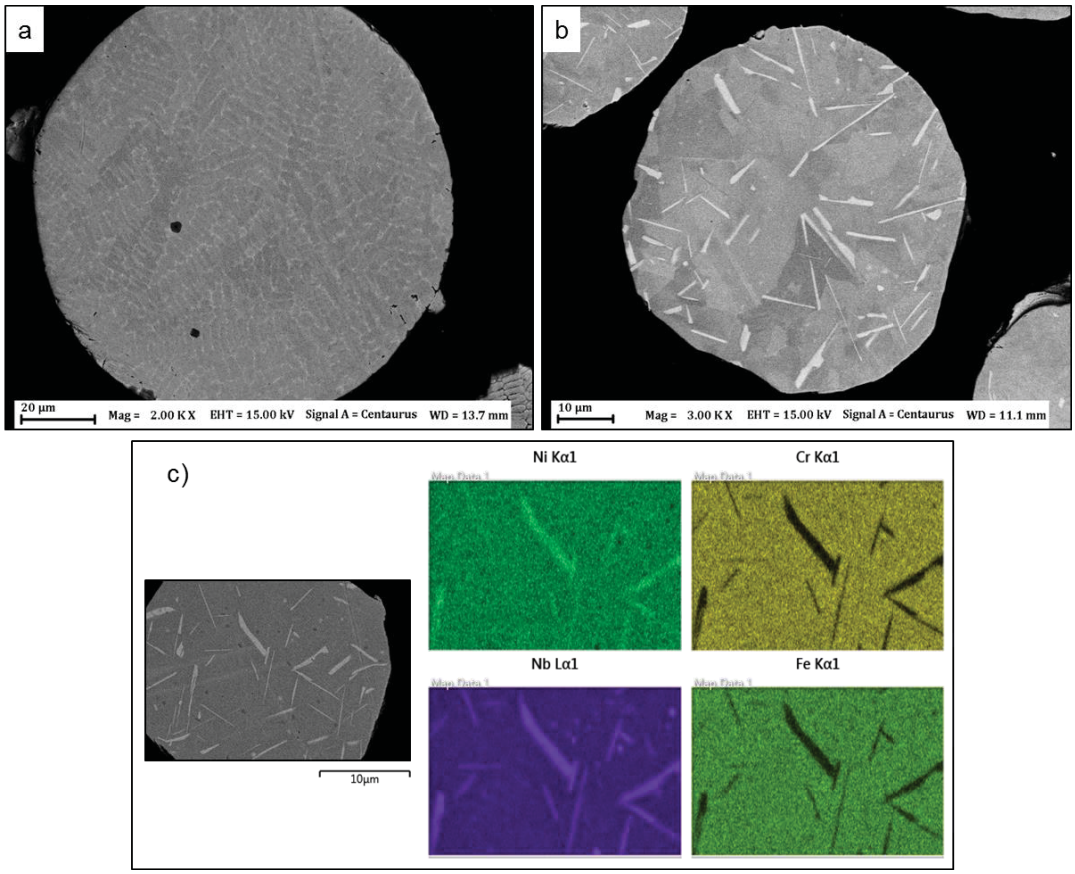

Fig. 9. Microstructure of Alloy 718 EBM powder in a) virgin condition; b) after 14 re-use cycles; c) EDS map showing delta phase in a powder after 14 re-use cycles. Author's experimental result.

4. DEFECTS IN ADDITIVE MANUFACTURED SUPERALLOYS

Porosity, micro-cracks and detrimental phases, such as non-metallic inclusions and unwanted secondary phases, are all defects commonly encountered in PBF fabricated parts [12]. Depending on their size, shape and distribution, they may act as potential failure initiation sites and may therefore have a negative influence the performance of AM parts. It should also be noted, however, that relative densities in the order of 99.9% [13] are commonly reached for many materials with today's PBF technology and that mechanical properties are often reported to be equal to, or in some cases even in excess of those for conventionally processed counterparts [13, 49].

Porosity has different origins and is divided into different groups such as gas porosity, shrinkage porosity and lack of fusion defects (LOFDs) [50]. Gas porosity, see Fig. 10 (a), consists of small, near-spherical pores which contain gas that is trapped in the metal during solidification of the melt pool, often arising from gas entrapped inside the powder during gas atomization [12, 50, 51]. The LOFDs, see Fig. 10 (b), are still to a large extent connected to the volumetric energy input and form in un-melted zones in the powder bed [11]. This defect type can also be connected to powder recycling and will be explained in more detail in the following section.

Presence of micro-cracks, see Fig. 10 (c), is largely connected to metallurgical reactions and is therefore an alloy-specific problem mainly present in so called "difficult-to-weld" materials [11]. Both non-metallic inclusions and unwanted secondary phases, Fig. 10 (d) and (e), respectively, are also to a large extent connected to the alloy chemistry and form either due to extensive segregation of certain alloying elements or due to reactions between reactive alloying elements (e.g. Al, Ti) and trace elements, such as oxygen and nitrogen [12].

An important consideration is the fact that porosity and cracks can in many cases be reduced or eliminated by applying a post-AM hot isostatic pressing (HIP) [12, 49, 51]. This is generally not the case though for non-metallic inclusions such as oxides and nitrides which, due to their high thermal stability, are largely unaffected by post-AM thermal processes [3].

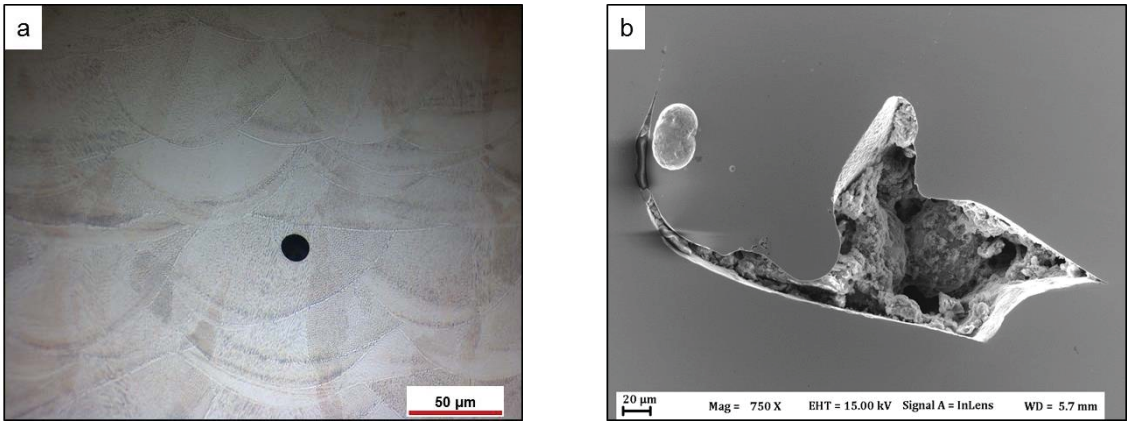

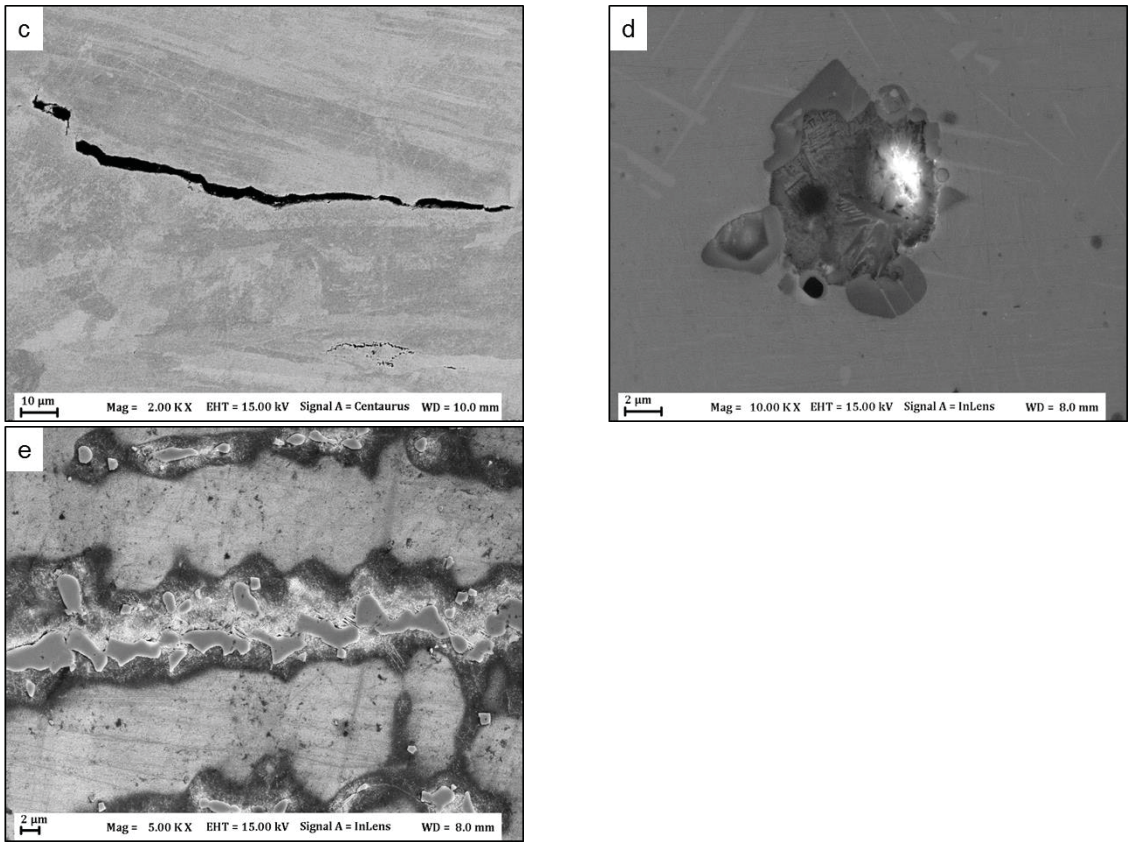

Fig. 10. Defects commonly observed in AM parts. a) gas porosity in 316L fabricated by LPBF; b) lack of fusion defect in EBM Alloy 718; c) micro-crack in precipitation strengthened Ni-base superalloy fabricated by LPBF; d) non-metallic inclusion (Al-oxide/Ti-nitride) in EBM Alloy 718; e) laves phase in Alloy 718 fabricated by wire DED. Author's experimental result.

4.1 Defects in EBM processed Alloy 718

Except for micro-cracks, EBM processed Alloy 718 contains all of the above mentioned defects to some extent. Oxide inclusions are commonly observed - often together with LOFDs close to the contour region, but also in the hatch region. Shrinkage porosity is mainly observed in the hatch region. Furthermore, presence of non-metallic inclusions and LOFDs stands in close relation to the powder oxygen level, which increases with progressive powder recycling, and requires a more careful description below.

4.1.1 Non-metallic inclusions

Non-metallic inclusions (NMIs) are compounds of metallic and non-metallic elements (usually O, S, N) present in the metal matrix [52]. NMIs are known to have a profound negative effect on mechanical properties, especially on the reliability of rotating parts [53]. For example, it has been shown that component life in both wrought and cast parts is often limited by fatigue failures often initiated at oxide inclusions [2]. NMIs are also a major cause for rejection of rotating part forgings [54]. Furthermore, the size of damage relevant inclusions is too small to rely on non-destructive testing alone, which can only detect relatively large inclusions [3].

Formation and stability

Based on their origin, NMIs are often divided into exogenous and endogenous inclusions. Exogenous inclusions originate from external sources such as fragments of refractories and entrapped slag, while endogenous inclusions occur due to chemical reactions between elements in the molten metal. Although mainly studied in casting, the latter is an intrinsic problem during

melting of alloys which contain reactive elements and may therefore occur in any other liquid metal process, such as powder atomization, welding and additive manufacturing. Endogenous NMIs form as a consequence of the strong tendency of reactive elements (such as Al and Ti) to form chemical compounds with non-metallic elements, such as oxygen, nitrogen and sulphur. This makes the solubility of these elements (i.e. the solubility product of the compound) extremely small in the metal matrix [55]. The solubility product is strongly temperature dependent and therefore, NMIs precipitate upon cooling of the melt when the concentrations exceed the solubility product of the compound [56].

There are two major types of NMIs in Alloy 718: titanium nitride (TiN) and aluminium oxide (Al_2O_3) [57]. The primary carbide NbC also precipitates in the melt but is usually considered as a part of the alloy microstructure [57]. As shown in Table 2, both O and N have very low solubilities, which means that extremely low levels are required to avoid formation of NMIs. Especially the oxygen level must be reduced to extremely low levels to avoid formation of oxide inclusions [54]. Furthermore, also for very low O and N levels, precipitation is expected well above the solidus temperature. Therefore, the population of NMIs can only be modified during the melting process while it is more or less unaffected by subsequent heat treatments.

Table 2. Solubility limits of O and N in Alloy 718 at the liquidus and solidus temperature [19]

Element	Solubility limit at T_L (ppm)	Solubility limit at T_S (ppm)
N	37	5
O	5	2

The size of NMI defects however, can be reduced by lowering the O and N levels to avoid precipitation until quite late in the solidification process. For both cast and wrought superalloys this is achieved first by primary melting in vacuum (VIM) in which the levels are lowered primarily through interaction with carbon to form CO (carbon boil) which is then desorbed by the vacuum. In this way, oxygen levels in the 20 ppm range are achievable [2]. Further reduction is made possible by applying one or several re-melting steps, including electroslag re-melting (ESR), vacuum arc re-melting (VAR) or electron beam cold hearth re-melting (EBCHR). The latter, which relies on dissociation and desorption (vacuum refining) and physical separation of inclusions which float to the melt surface, has been shown to be very promising for removal of impurities and inclusions [53, 54]. In this manner, single ppm oxygen levels has long been attainable in the superalloy casting industry [54]. A typical value for wrought counterparts Ni-base superalloys is usually around 20 ppm [12, 54].

NMIs in the powder production and PBF

The O and N levels commonly observed in the Alloy 718 atomization precursor wire, EBM powder (virgin and re-used) and EBM fabricated solid samples investigated in this thesis study are listed in Table 3. For all material conditions, the oxygen and nitrogen levels are well above the solubility limits in Table 2 and therefore, some amount of Al_2O_3 and TiN is expected. However, while many studies have been addressed to microstructural characterization, those dedicated to non-metallic inclusions, like that of Polonsky et al. [12], are very scarce. Due to the high temperature under the electron beam (which has been reported to be around 3000°C [19]), it is suggested that dissolution of NMIs takes place during EBM. Similar effects have also been suggested to occur during plasma atomization, which also takes place at very high temperature. However, it is also known that stable non-metallic phases may persist through both powder production [2] and electron beam melting [3].

Table 3. Oxygen and nitrogen levels in the Alloy 718 wire, powder and solid samples investigated in this study

Material	O (ppm)	N (ppm)	C (ppm)
Wire	~75	~150	~440
Powder - virgin	~150	~150	~370
Powder - re-used	~300	~150	~370
Solid – virgin	~75	~150	~300
Solid - re-used	~150	~150	~300

Furthermore, the solvus temperature is composition dependent and increases with analytical content of the elements in the compound. Following this concept, the calculated solvus temperatures for Al_2O_3, TiN and NbC based on an average composition of re-used Alloy 718 powder (Table 3) are shown in Table 4. Among these phases, Al_2O_3 is present at the highest temperature, followed by TiN and finally NbC which precipitates slightly above the solidus temperature. These values are all lower than the peak temperature reported for EBM. However, it should be noted that, even though the temperature in these processes may be high enough for dissolution to take place, the high solidification rate limits the residence time at high temperature necessary for dissolution [2, 58].

*Table 4. Solvus temperatures for TiN and Al_2O_3 in Alloy 718 calculated with JMatPro. *The dissolution temperature is composition dependent and is in this case based on average O, N and C levels in the re-used powder (250 ppm O, 150 ppm N, 370 ppm C), see Table 3*

Phase	Solvus temperature* (°C)	Melting temperature (°C)
NbC	1260	3490
TiN	1640	2930
Al_2O_3	2050	2030

The nitrogen level in Table 3 is stable at around 150 ppm for all material conditions, which indicates that the amount of TiN is stable during powder production, powder recycling and electron beam melting. Furthermore, all three material conditions contain very similar TiN particles with sizes varying from sub-micron up to around 10 μm. In many cases, they are found to consist of an Al_2O_3 core and an outer TiN rim, see Figs. 11 and 12. Both powder atomization and EBM are associated with rapid solidification rates and therefore there is limited time for particle growth. In this respect, the morphology of the TiN/Al_2O_3 particles, which is similar for all material conditions, suggests that at least the larger inclusion sizes of the population of TiN particles are most likely inherited from the atomization precursor material, i.e. from the wire.

The wire also contains relatively large primary NbC carbides, see Fig. 11. In some cases they are nucleated on the TiN particles. Such structures are not seen in the powder or in the solid samples. This indicates that the temperature during atomization is high enough to dissolve NbC (which is the least stable phase according to Table 4). The continuously decreasing carbon level along the process chain from wire to powder and finally EBM processed solid suggests that some amount of carbon is removed during both atomization and EBM processing, while the remainder re-precipitates upon cooling [55].

It should be noted that the observed oxide-nitride-carbide particles are well known to exist in various metal systems. The structure corresponds to the sequence of nucleation of these phases in the melt (according to the solvus temperatures in Table 4), starting with Al_2O_3, followed by TiN and finally NbC [19].

As a consequence of oxygen pick-up during powder production, the powder oxygen level is higher than in the wire. Moreover, the amount of oxide increases significantly during powder re-use as already described in section 3.2.2. The oxygen level in the solid samples is around half compared to the powder from which it was built, which shows that some amount of oxide refining takes place during the EBM process.

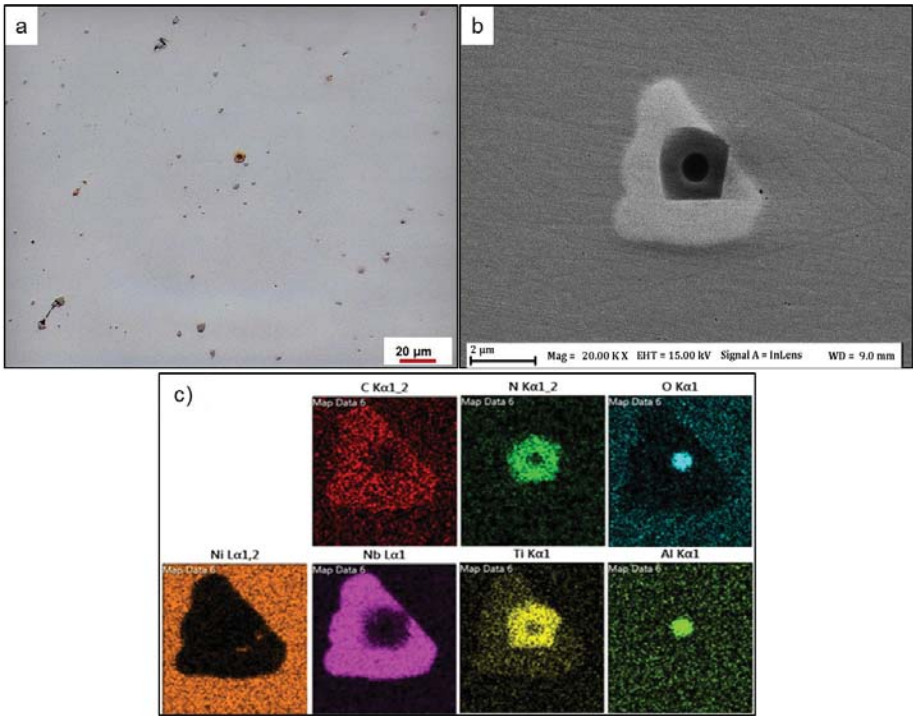

Fig. 11. NbC/TiN/Al_2O_3 particle in the Alloy 718 wire (atomization precursor material) with corresponding EDS map in (c). Author's experimental result.

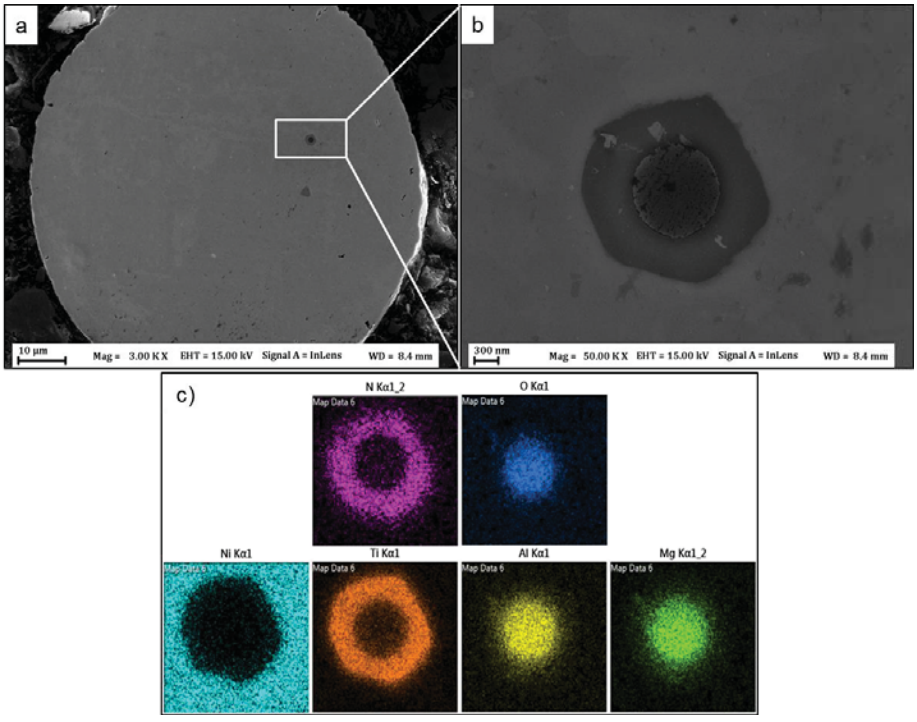

Fig. 12. TiN/alumina particle in a plasma atomized Alloy 718 virgin powder with corresponding EDS map in (c). Author's experimental result.

In the EBM fabricated samples, oxide exists both as particulates and as continuous films or flakes, see Fig. 13. As will be described below, its tendency to agglomerate in the melt results in the formation of such large NMIs. This is especially the case in samples fabricated from re-used powder, where the increased amount of oxide is the major source for NMIs.

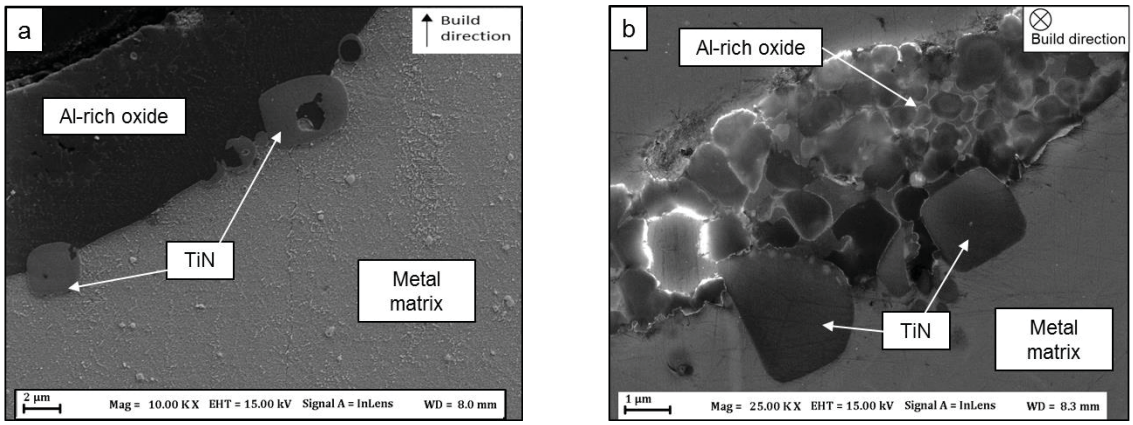

Fig. 13. EBM processed Alloy 718 a) TiN inclusions in an oxide flake in a sample built from 30 times re-used powder; b) clustered TiN and oxide inclusions in a sample built from 14 times re-used powder. Author's experimental result.

Agglomeration of non-metallic phases

Agglomeration of NMIs in the liquid melt is a phenomenon well-known in the casting industry [59]. In case of sub-micron inclusions, it is reported to be a result of collision which is mainly governed by the turbulence present in the melt [60]. Collision and agglomeration of single alumina particulates is promoted by long-range attraction forces [59]. When inclusions collide, they tend to coalescence or agglomerate if the interfacial tension between particle and melt is high [61]. In EBM processed Alloy 718, oxide particulate clusters with size of several tens of µm are frequently present in samples produced from re-used powder, see Fig. 14. The individual oxide particulates have size and shape similar to those on the surface of the re-used powder, see Fig. 8. This suggests that they persist the melting process and cluster in the molten metal. No such clusters were observed in samples produced from virgin powder.

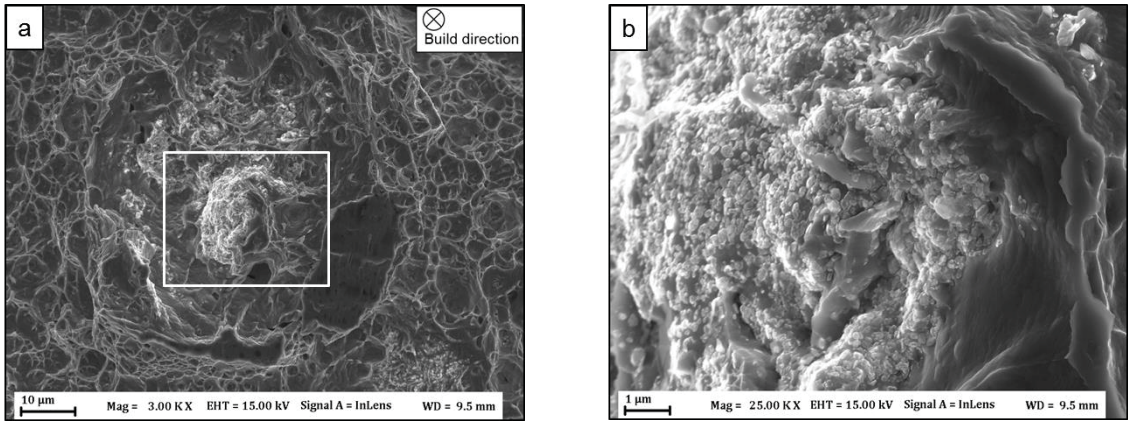

Fig. 14. Cluster of Al-rich oxide inclusions in an EBM Alloy 718 sample fabricated from 14 times re-used powder. Author's experimental result.

Similar phenomena, apparent in LPBF, is shown in Fig. 15, where equally sized TiN particles are present both in the atomized Alloy 718 powder, Fig. 15 (a), and in the fabricated solid sample, Fig. 15 (b). In this case, melting of the raw material as well as atomization was done in a nitrogen atmosphere which enables TiN formation through reaction with Ti in the melt before atomization.

Also in this case, the inclusions in the AM part are found as agglomerates in the solid sample which indicates that particulate agglomeration occurs in the melt, as reported in earlier studies [3, 12, 62]. As mentioned in section 3.1.3, similar phases can also originate from entrapped refractory material from the crucible and/or nozzle in the atomizer [63].

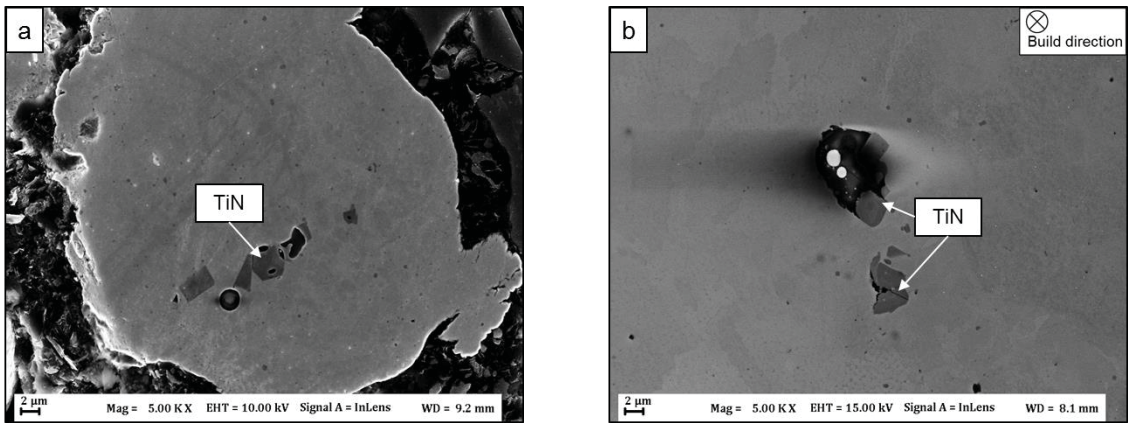

Fig. 15. TiN particles in (a) gas atomized Alloy 718 powder and in (b) the solid sample fabricated by LPBF. Author's experimental result.

Large inclusions are mainly composed of agglomerates as a consequence of the macroscopic melt flow, a process which is more effective when the phases are in liquid state [60]. As the melting temperature of Al_2O_3 (~2000°C) can easily be reached in EBM, this may result in formation of large continuous oxide films/flakes, as shown in Fig. 16. The oxide often incorporates nitride particles which together form large, brittle defects. This effect is especially seen in samples produced from re-used powder where both number density and size of these NMIs is considerable. Similar oxide inclusions have previously been observed in EBM processed Alloy 718 [19]. Oxide inclusions present in LPBF and DED are usually reported to form mainly due to pick-up of oxygen from the processing atmosphere [64, 65].

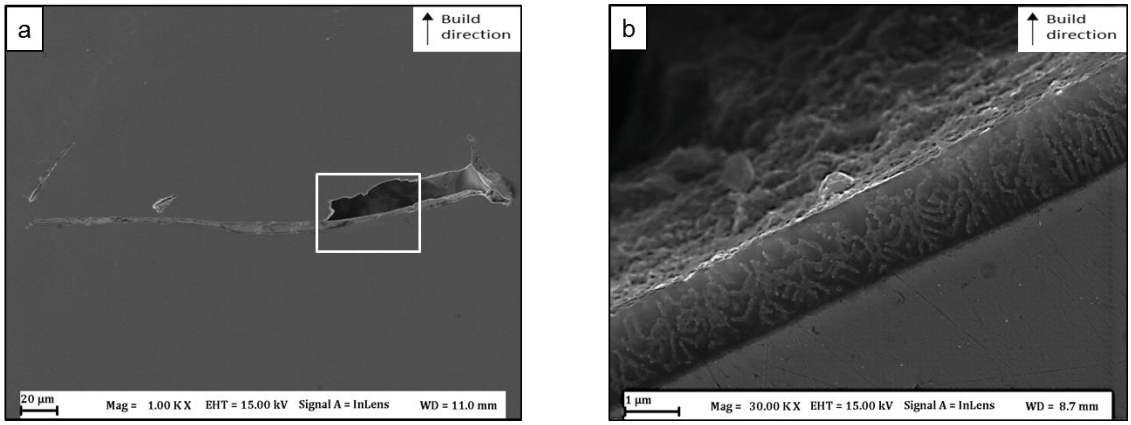

Fig. 16. Large oxide flake in an EBM processed Alloy 718 sample built from 30 times re-used powder. Author's experimental result.

Floatation of non-metallic phases

Flotation of many NMIs is natural to occur through buoyance effects since the density is often lower than that of the molten metal (3.95 g/cm^3 for alumina and 5.4 g/cm^3 for TiN in comparison to 8.22 g/cm^3 for Alloy 718). In casting, this process is reported to be more efficient for larger particles and is limited to inclusions above 30 µm [59]. For EBM however, it has been claimed that the solidification rates are too high for effective buoyancy forces to occur. Instead, thermocapillary (Marangoni) forces, as illustrated in Fig. 17, are assumed to be the major mechanism for flotation of non-metallic phases [12].

Marangoni flow is driven by large thermal gradients and consequently a large surface tension gradients across the melt pool surface. When the level of surface active elements such as O and/or S exceeds around 10 ppm, the surface tension temperature dependence changes from positive to negative, as illustrated in Fig. 17. This has the effect that the particle trajectory is directed radially inwards towards the hotter region at the top centre of the melt pool. Hence, as a consequence of layer re-melting, NMIs may be transported from layer to layer along the building direction towards the part top surface. A large amount of oxide on the top surface of a sample built from re-used powder, Fig. 18 (a-c), confirms that this is the case. This also shows that some amount of refining of the bulk material takes place, which is one reason for the lower oxygen level in the bulk solid sample compared to the powder from which it was built. However, the oxide may also become entrapped into the melt due to the turbulence, forming the defects shown in Fig. 18. Similar inclusions, so called oxide bi-films, are also formed due to turbulence during casting of Ni-base superalloys [66]. The lower amount of oxide in the samples produced from virgin powder is confirmed by an almost complete absence of oxide on its top surface, as shown in Fig 18 (d).

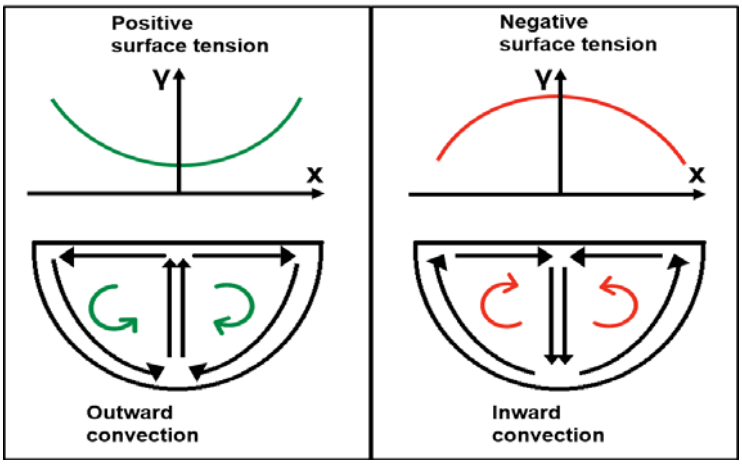

Fig. 17. Illustration of the Marangoni effect on the trajectory of particles in a melt pool. Redrawn from [1].

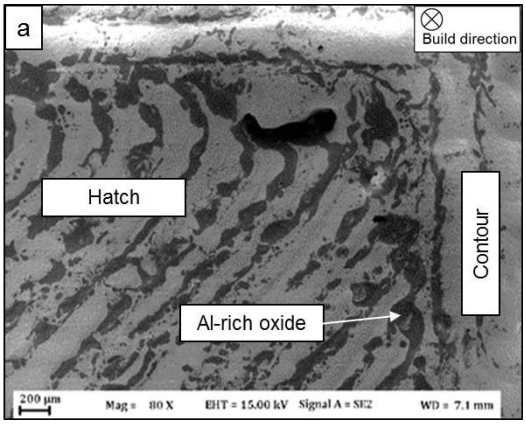

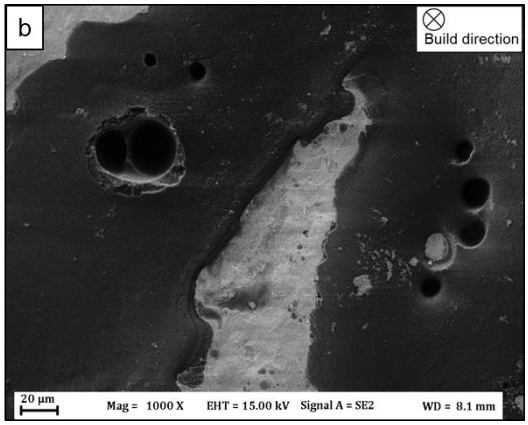

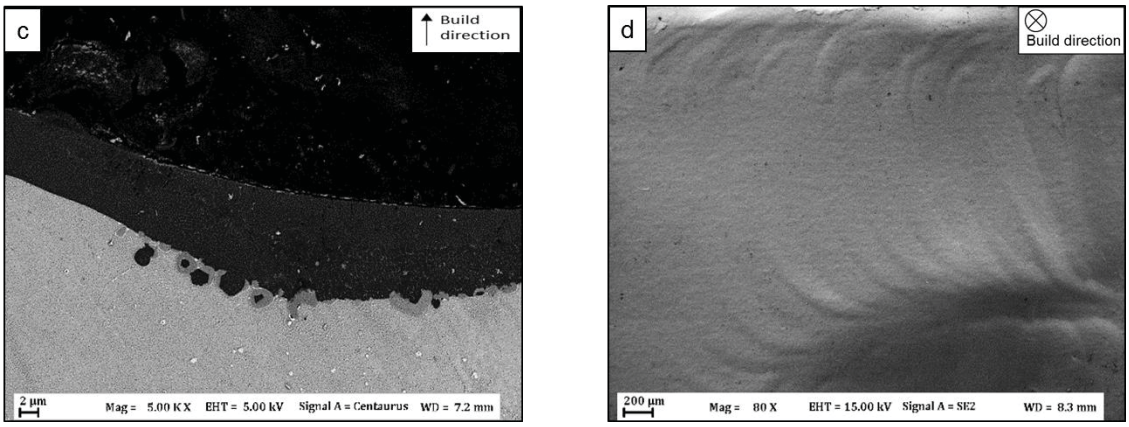

Fig. 18. (a-c) Top surface of EBM processed Alloy 718 built from 30 times re-used powder; (a-b) top view; (c) cross section; (d) top view of sample built from virgin powder. Author's experimental result.

4.1.2 Lack of fusion defects

Lack of fusion defects (LOFDs) occur when the overlap between adjacent melt pools is insufficient. Generally speaking, the presence of LOFDs is largely process dependent and typically occurs when using non-optimized process parameters or due to anomalies in the process such as a temporary decrease in beam power and/or irregularities in the thickness of the powder layer [12]. In EBM processed Alloy 718, LOFDs are especially found at the interface between the hatch and contour region, as shown in Fig. 19, for which the reason is twofold.

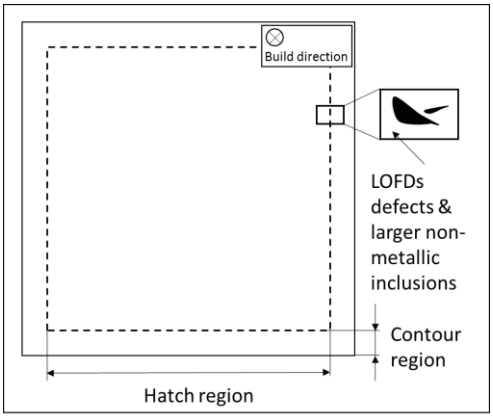

Fig. 19. Predominant position of LOFDs at the interface between the hatch and contour regions in EBM processed Alloy 718. Author's illustration.

Firstly, as the electron beam follows the hatch scan pattern, see Fig. 2, excessive melting may take place at the turning points, resulting in the formation of a crater in this particular area. In such a case, the successive powder layer is locally too thick to reach full consolidation. Hence, stacking of LOFDs defects in the z-direction may occur in this particular region, as shown in Fig. 20 (a).

Secondly, as can be seen on the top surface of the samples built from re-used powder in Fig. 18 (a), large amounts of oxide is accumulated at the electron beam turning points. As oxide is known to negatively affect the wetting process, this leads to a further increased risk of LOFD formation [64]. An increased number of LOFDs in samples produced from re-used powder, together with large amounts of oxide inside the LOFDs, see Fig. 20 (b-d), confirms this theory. Similar observation have been done in other studies [62].

In addition, the oxidized surface of the re-used powder could possibly lead to a reduced energy absorption and/or powder bed conductivity. This may have a negative effect on the sintering behaviour and therefore ejection of powder (powder smoking), with the formation of LOFDs in the subsequent layer as a result [12].

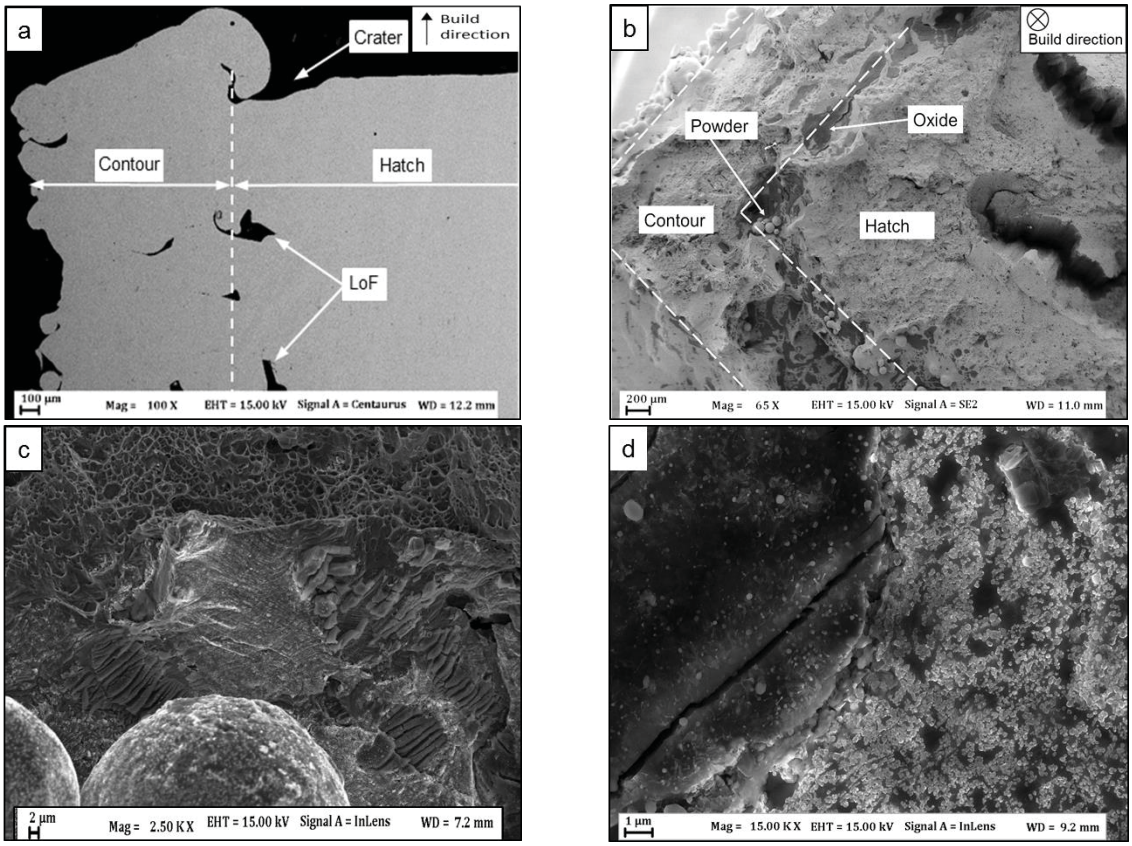

Fig. 20. LOFDs present at the interface between the hatch and contour regions in an EBM processed Alloy 718 sample fabricated from re-used powder a) cross section parallel to the build direction; b) fracture surface perpendicular to the build direction; c)-d) higher magnification of oxidized powder inside and oxide films/flakes inside LOFD in b). Author's experimental result.

Furthermore, oxide containing LOFDs in samples built from re-used powder cannot be eliminated with hot isostatic pressing. Instead, after HIP, large networks of oxide remains inside the collapsed LOFDs, see Fig. 21.

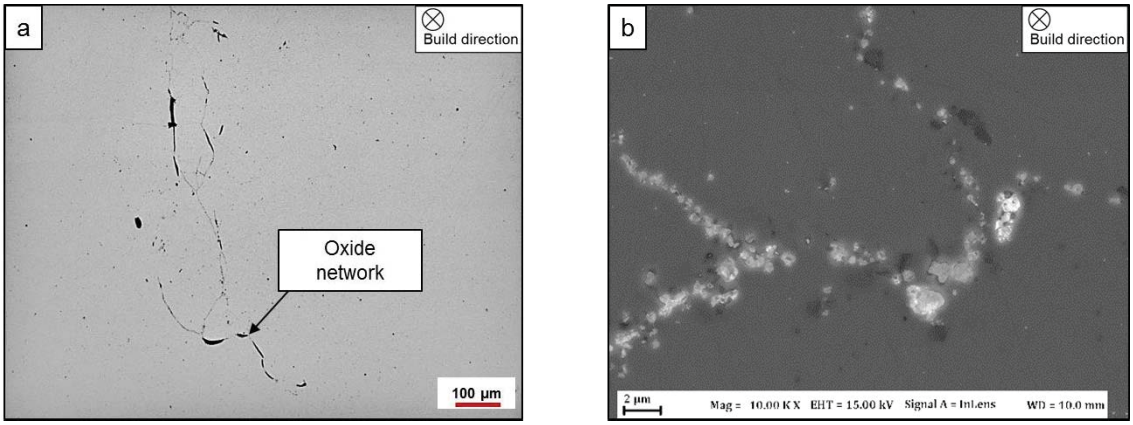

Fig. 21. Network of Al-rich oxide inside a collapsed LOFD in an EBM processed Alloy 718 sample fabricated from re-used powder. Author's experimental result.

5. EXPERIMENTAL PROCEDURE

In this study, virgin and re-used Alloy 718 EBM feedstock powder was analysed to determine the influence of multi-cycle EBM processing on the powder chemistry and surface morphology. Solid samples produced from virgin and re-used powder were studied to determine the effect of powder recycling on the presence of defects in EBM fabricated parts.

5.1 Material

Commercial Alloy 718 pre-alloyed powder was used as feedstock material in the EBM process. The powder was produced by plasma atomization of a wire precursor material in an argon atmosphere. The virgin powder was provided by Arcam AB, Sweden and had a particle size distribution of 45-105 μm. Its chemical composition, presented in Table 5, complies with common Alloy 718 material standards such as AMS 5662. The oxygen and nitrogen levels in the virgin powder, as measured by inert gas fusion (see below), were both in the order of 150 ppm.

Table 5. Chemical composition of the Alloy 718 powder as provided by the powder producer

Element	Ni	Co	Cr	Mo	Ti	Mn	Nb	B	P	Ta	Al	Fe	Si	S	C
wt.%	54.1	0.04	19.0	2.99	1.02	0.12	4.97	0.001	0.004	<0.01	0.52	17.12	0.06	<0.001	0.03
at.%	53.38	0.04	21.16	1.80	1.23	0.13	3.10	0.01	0.01	<0.01	1.12	17.75	0.12	<0.001	0.14

An ARCAM A2X EBM system, located at University West, Trollhättan, Sweden, was used to fabricate the solid samples. The EBM machine was run using a 4.2 version control software. The samples were built using Arcam standard process parameters and melt strategies, using an acceleration voltage of 60 kV and a layer thickness of 75 μm.

An approximately 1 mm wide area around the sample edges were first built up by applying 3 contour passes with a line offset of 300 μm. This was followed by a bi-directional hatch exposure at the sample core with a line offset of 125 μm. The hatch passes were rotated by 60° between each layer. The samples had a geometry of 11x11x60 mm^3 and were built with the longitudinal direction parallel to the build direction. Standard Charpy V-notch (CVN) test bars with a geometry according to ASTM standard E2316-b were machined from the samples. Hot Isostatic Pressing (HIP) of the solid samples was performed at a temperature of 1200°C, applying pressure of 1000 bar for 4 hours.

The samples were built in four sequential build cycles. The first cycle was started with 100 kg of virgin powder from which the first sample set was produced. The following two sets were produced in cycles 6 and 14, using the same powder batch. Up to cycle 14, addition of virgin powder was kept as low as possible and was limited to cycle 6 before which 20% was added. The last set was produced from a mixture of heavily recycled powder, which had been exposed to up to 30 times of powder recycling corresponding to a total process time of around 1000 hours.

Samples of the re-used powder were collected before as well as after the above mentioned EBM build cycles. Powder sampled from the sintered cake surrounding the built components shows the effect of exposing the powder to the conditions in the EBM process chamber. The samples collected before filling the powder into the powder hoppers (after sieving) show the overall condition of the powder used for sample fabrication. These samples were studied together with the solid samples built from the powder in question.

5.2 Analysis techniques

The surface sensitive analysis methods X-ray photoelectron spectroscopy and Auger electron spectroscopy were used in combination with scanning electron microscopy to depict the differences in surface morphology, chemical state and surface composition of the powder samples exposed to varying numbers of re-use cycles. The EBM fabricated samples produced from virgin and re-used powder were studied in terms of defect density as well as defect distribution. The defect morphology in solid samples was studied to understand its origin and formation mechanism. The amount of non-metallic inclusions in powder and solid samples was estimated from bulk chemical analysis.

Scanning electron microscopy

The scanning electron microscope (SEM) is a very useful and versatile instrument that is often used for morphological as well as elemental analysis. Secondary electrons (SE) originate from the near-surface region and are therefore used for high resolution imaging of the surface topography. The backscattered electrons yield is dependent on the atomic number, which is widely used for determining the compositional contrast in the sample. Moreover, by detecting differences in the phase conductivity (work function), the SE in-lens detector allows for enhanced phase contrast compared to a conventional secondary electron detector. Emission of characteristic X-rays upon interaction with the electron beam is used for micro-chemical analysis by energy dispersive X-ray spectroscopy (EDS). The spatial resolution of EDS is influenced by the interaction volume which depends on the accelerating voltage and also on the density of the sample but is often in the order of a micrometre.

The surface morphology of the virgin and re-used powder was characterized using a Leo Gemini high resolution scanning electron microscope (LEO GmbH, Oberkochen, Germany) equipped with a secondary electron in-lens detector. A solid-state EDS detector from Oxford Instruments (X-Max, Oxford Instruments Ltd., High Wycombe, UK) connected to the SEM was used for qualitative analysis of the phases present on the powder surface and on the powder cross sections.

Fractography of solid samples was performed by means of SEM to study the morphology of defects in samples produced from powder exposed to varying extent of powder recycling. As part of the characterization of the defects and their distribution, selected cross sections of the sample interior and the top surface was studied in terms of amount of non-metallic phases together with their location relative to the solidification structure (melt pools) of the last solidified layer. EDS was used for qualitative micro-chemical analysis.

Auger electron spectroscopy

As compared to SEM/EDS, Auger electron spectroscopy (AES) is a surface sensitive technique which offers the possibility to perform laterally resolved surface chemical analysis with a nominal analytical lateral resolution of 10-20 nm and an interaction depth of 0.5-5 nm below the sample surface. Together with the electron imaging capabilities, AES enables semi-qualitative analysis of small surface features. Argon ion etching capabilities of the system allows for chemical depth profiling.

Powder analysis by SEM/EDS was complemented by AES using a PHI700 instrument from Physical Electronics (Chanhassen, Michigan, USA) for detailed local characterization of oxide particulates on the surface of the re-used powder.

X-ray photoelectron spectroscopy

X-ray photoelectron spectroscopy (XPS) is a technique for investigating the elements at solid surfaces, their concentration and chemical state by determination of the characteristic binding energy of photoelectrons that are emitted from the sample when irradiated with X-rays. Due to its ability to detect the chemical state of the elements, XPS is a valuable tool for gathering detailed information about the sample surface chemistry. The analysed photoelectrons originate from the top 1-10 nm of the surface.

Surface chemical analysis of virgin and recycled powder was performed by means of a PHI 5500 instrument to depict the differences in chemical state and surface composition of powder samples exposed to varying numbers of re-use cycles. The photoelectrons originated from an area of around 0.8 mm in diameter (~100 particles) which means that the signal represents the overall chemistry of the analysed powder surface. Survey spectra were recorded for identification of elements present on the powder surface. Narrow scan energy regions corresponding to the elements of interest were then selected for detailed analysis followed by peak identification and curve fitting using the software PHI Multipak to obtain the chemical composition of the surface and the chemical state of the elements. Surface compound thicknesses and chemical composition in-depth distribution from the as-received surface down to an etch depth of 500 nm were obtained by altering XPS analysis and argon ion etching. The fraction of the oxide forming elements in cation state (i.e. oxide or hydroxide) along the depth from the as-received surface was determined from peaks curve fitting of the XPS high resolution spectra.

Defect density measurements

Quantification and distribution of non-metallic inclusions in samples built from progressively re-used powder was measured by metallographic image analysis of light optical microscopy images. Defect quantification in the hatch and contour regions was evaluated on cross sections transversal to the build direction. Similarly, distribution of defects in the Z-direction was determined by evaluating cross section located at different positions along the build direction, as shown in Fig. 24 (a) and (b). The total amount of defects (porosity and non-metallic inclusions) was analysed in samples in as-printed condition. Quantification of non-metallic inclusions was done after hot isostatic pressing (HIP), which eliminates porosity and lack of fusion defects. HIP was done at 1200°C, 1000 bar for 4 hours.

Bulk chemical analysis

The inert gas fusion technique (often referred to as combustion analysis) is used to measure the oxygen, nitrogen and hydrogen content in inorganic materials. In this process, a sample placed in a high purity graphite crucible is fused at a high temperature (roughly 3000°C) in a flow of inert gas. The oxygen present in the sample reacts with carbon from the graphite crucible to form carbon monoxide (CO) and carbon dioxide (CO_2), whereas nitrogen and hydrogen are released as gas molecules (N_2 and H_2). The combustion gases are carried with inert gas flow onto a detector where it is measured [67].

Oxidation of the non-consumed, re-used powder as a consequence of progressive powder recycling was mapped by measuring the oxygen level of powder samples collected in the sintered powder cake after build cycle completion. Similarly, the oxygen level of the powder before starting the build cycles was compared to the oxygen level of the corresponding solid samples to find the correlation between oxidation of the re-used powder and the amount of oxide inclusions present in the solid samples.

Furthermore, distribution of oxide and nitride inclusions along the build direction as well as in the XY-direction, as described above, was complemented by oxygen and nitrogen levels measured in samples extracted from different positions within the solid samples, as shown in Fig. 24 (c).

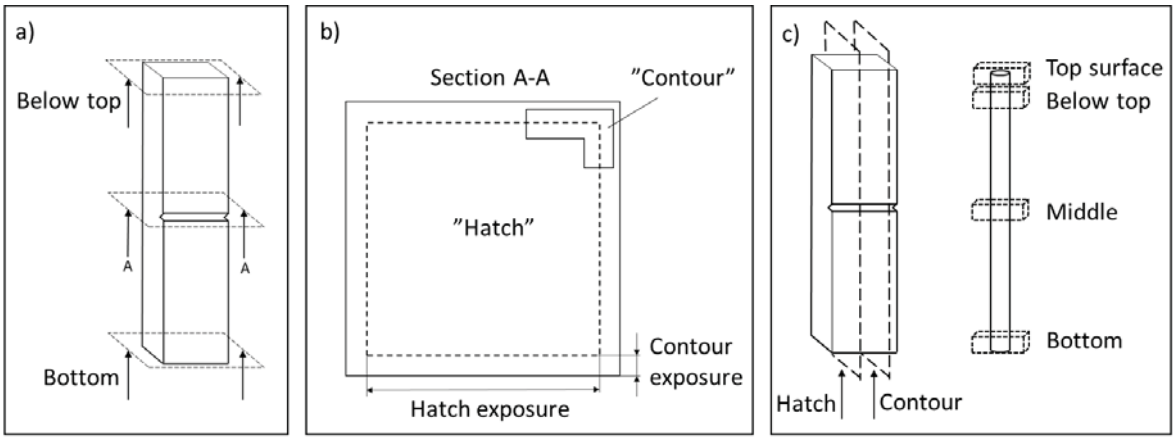

Fig. 22. Sample positions evaluated for a-b) defect density and c) oxygen and nitrogen measurements.

6. SUMMARY OF RESULTS IN APPENDED PAPERS

In **paper I**, virgin and re-used powder was studied to determine the influence of multi-cycle EBM processing on the surface morphology and chemistry of Alloy 718 powder. A significant change in the powder surface chemistry, as a consequence of exposing the powder to the conditions in the EBM process chamber, is observed, as illustrated in Fig. 23. The virgin powder surface, Fig. 23 (a), has a smooth and clean appearance that is visually free from non-metallic phases or other contamination species. The powder collected after build cycle 14, on the other hand, has a very different character in the sense that it contains a significant amount of oxide particulates that had formed on its surface, see Fig. 23 (b).

Based on the XPS and AES analyses of the two powder conditions presented in **paper I**, the transformation of the powder surface during multi-cycle EBM processing is illustrated in Fig. 23 (c). The virgin powder surface is covered by a relatively thin and homogeneous Ni- and Al-rich oxide/hydroxide layer. The prolonged exposure at high temperature (around 1000°C) in the EBM build chamber enables selective oxidation of aluminium, which resulted in formation of Al-rich oxide particulates. Significant growth occurs through aluminium diffusion from the powder interior together with pick-up of oxygen from the process environment. In addition, aluminium and oxygen are re-distributed from the less stable products such as Ni-oxide and/or hydroxide in the initial oxide layer to form the more stable Al-rich oxide. This transformation starts already during the first build cycle and tends to increase with progressive powder re-use. It results in a heterogeneous distribution of thermodynamically stable Al-rich oxide particulates, co-existing with a thin layer of transition metal oxide/hydroxide which is formed in the regions in-between the oxide particles, most likely during subsequent exposure to air at lower temperatures, including powder handling.

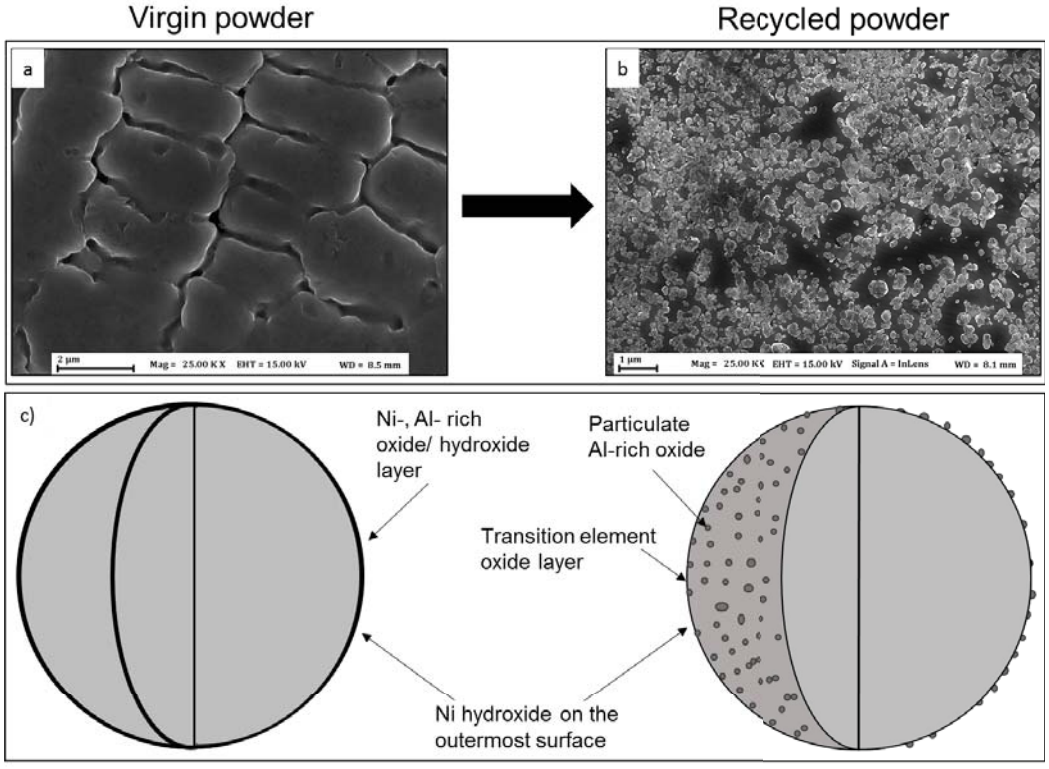

Fig. 23. Transformation of powder surface oxide layer during multi-cycle EBM processing; a) virgin powder; b) re-used powder collected after build cycle 14; c) illustration of the powder before and after re-use.

The observed oxidation of the powder surface, as a result of powder recycling, is confirmed by a continuously increasing powder oxygen level, as shown in Fig. 24. Furthermore, there is a clear correlation between the oxygen level in the solid samples and the powder from which they were built, which both increase with respect to progressive powder re-use.

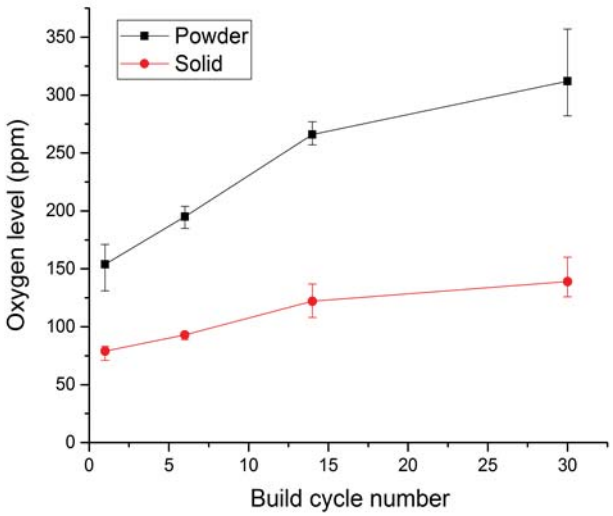

Fig. 24. Oxygen level in powder (before build) and solid sample bulk material with respect to powder re-use.

Fractography of samples built from virgin and 14 times re-used powder was performed in **paper II**. It was found that oxide inclusions are present on the fracture surfaces of samples built from both, virgin and re-used powder. As indicated in Fig. 24, the samples produced from re-cycled powder contain a larger amount of oxide inclusions as compared to those produced from virgin powder. In both cases, the largest oxide inclusions are found in the area between the hatch and the contour regions. The macroscopically rough surface topography in these regions is a result of such defects which constitute weak interfaces along which the crack front propagates through an intergranular type of fracture.

As shown in **paper III**, four different oxide morphologies were observed in the samples produced from re-used powder, see Fig. 25. Similar for all cases is the presence of oxide particulates with the same size and shape as on the re-used metal powder. The formation mechanism is largely connected to the melting process and depends on the ability of the electron beam to melt the oxide and the surrounding metal. This is dependent on the volumetric energy density and the residence time of the electron beam but also on the local wetting conditions, which is in this case reduced by presence of oxide beneath the powder layer. In case of a low degree of melting, the absence of a continuous melt pool results in oxide particulates dispersed inside LOFDs, as shown in Fig. 25 (a, b). With an increasing degree of melting, the oxide particulates are present as clusters in the metal matrix, see Fig. 25 (c, d). This is followed by a range of partially to fully melted, continuous oxide flakes, when the degree of melting is further increased as shown in Fig. 25 (e, f).

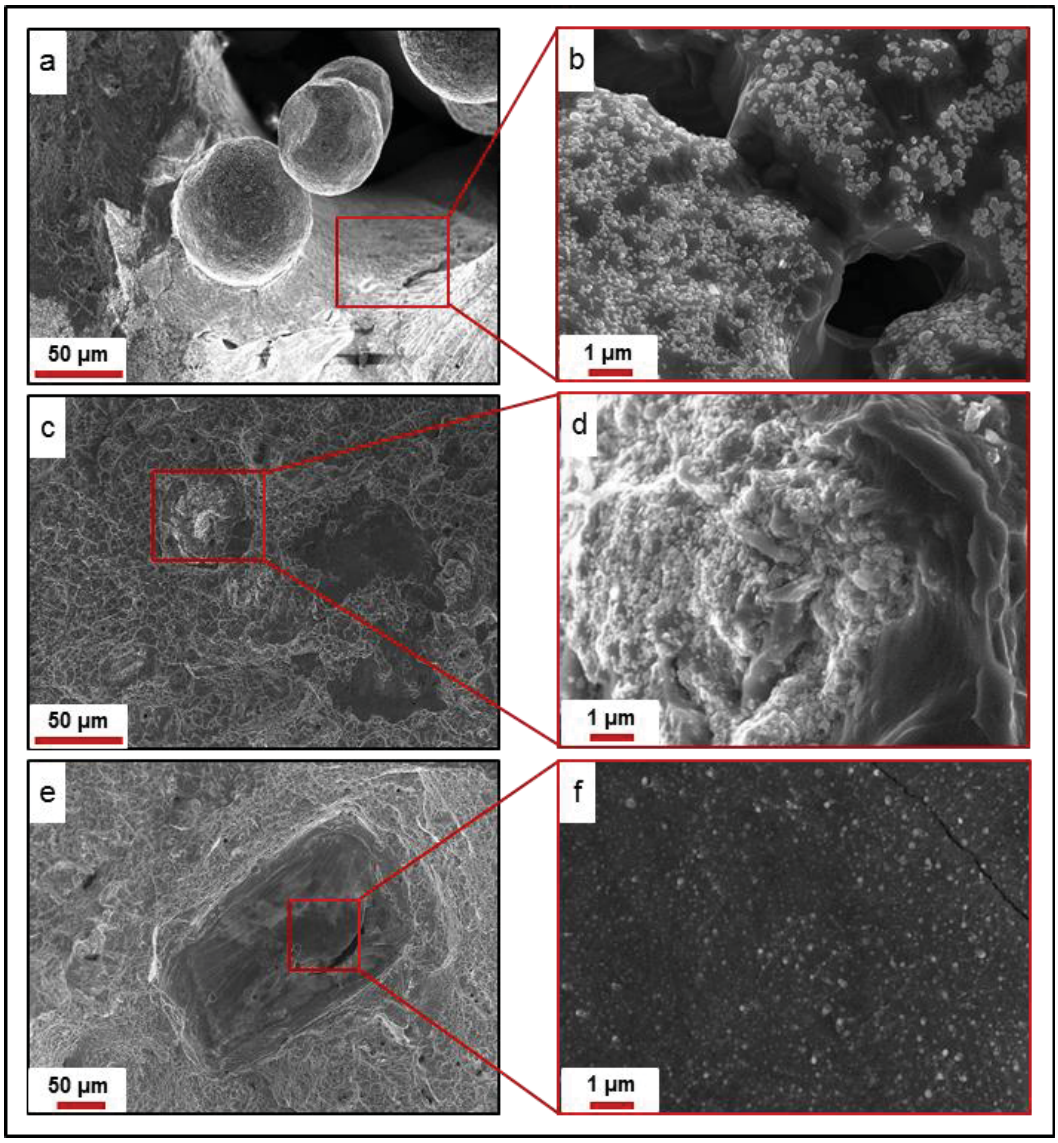

Fig. 25. Different oxide defect morphologies in EBM processed Alloy 718 built from re-used powder ranging from (a, b) dispersed particulates, (c, d) clustered particulates and (e, f) fully melted Al-rich oxide.

Based on the above observations, it can be concluded that a major part of the observed oxide inclusions originates from the Al-rich oxide particulates on the surface of the re-used powder. As illustrated in Fig. 26, due to its low solubility in the metal, this oxide persists the melting process and is transferred to the component without being dissolved. Agglomeration of the oxide in the molten metal may result in large aggregates, which are sometimes entrapped as large inclusions in the metal during solidification. TiN particles present in the powder also participate in the clustering and are commonly present at the metal/oxide interface.

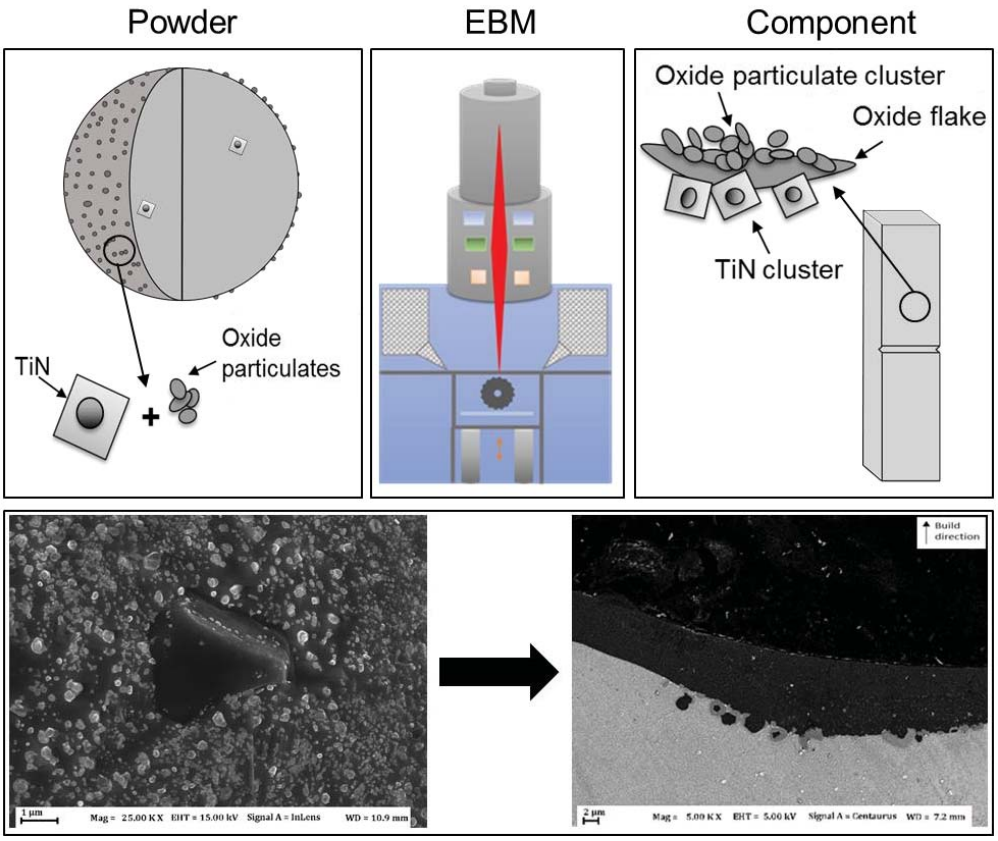

Fig. 26. Transfer of non-metallic inclusions from the powder to the component during EBM processing.

Quantification of defects and their distribution in solid samples produced from virgin and recycled powder was also studied in **paper III.** Metallographic image analysis shows a clear correlation between the amount of defects in the solid samples and the powder oxygen level as a consequence of progressive powder recycling. This is the case in both as-printed condition as well as after HIP consolidation, as shown in Fig. 27. The trend is especially clear in the contour region in as-printed condition due to an increased amount of LOFDs defects in samples produced from the re-used powder. In case of samples produced from virgin powder, hot isostatic pressing can be successfully used to reach a near fully dense material. However, for the samples fabricated from recycled powder, a considerable amount of oxide inclusions remains after HIP treatment, especially in the contour region, see Fig. 27 (b).

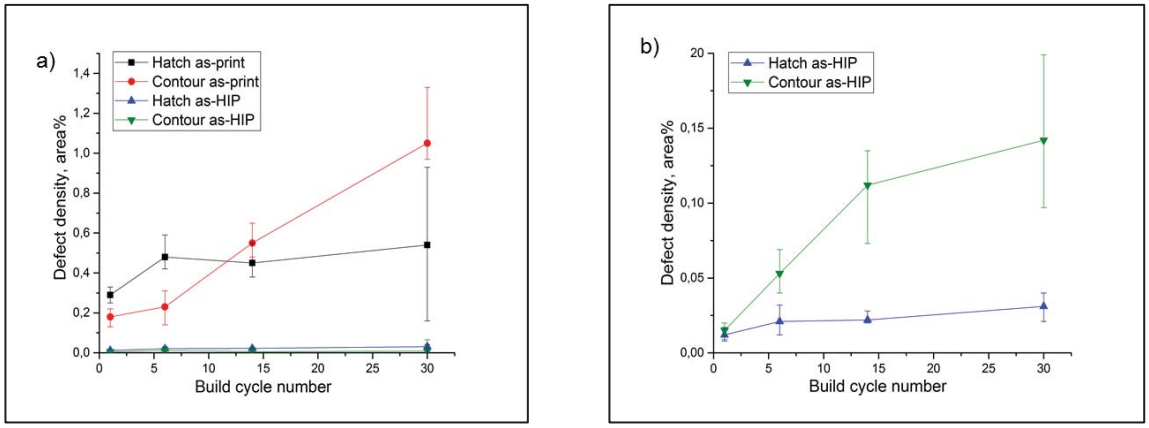

Fig. 27. Defect density in samples built from progressively re-used powder; a) as-printed and as-HIP condition; b) as-HIP condition.

Accumulation of oxide in the contour region is confirmed by considerably higher oxygen level as compared to the hatch region, as shown in Fig. 28. Similarly, the top surface also shows a clearly higher oxygen level than the bulk material value. Both of these trends can be explained by studying the sample top surface, as shown in Fig. 18 (a). In general, it is seen that the top surface contains a large amount of oxide, which is particularly concentrated in the area at the interface between the hatch and the contour region. This distribution of oxide in the solid samples is a function of transfer mechanisms along as well as perpendicular to the build direction, as illustrated in Fig. 29.

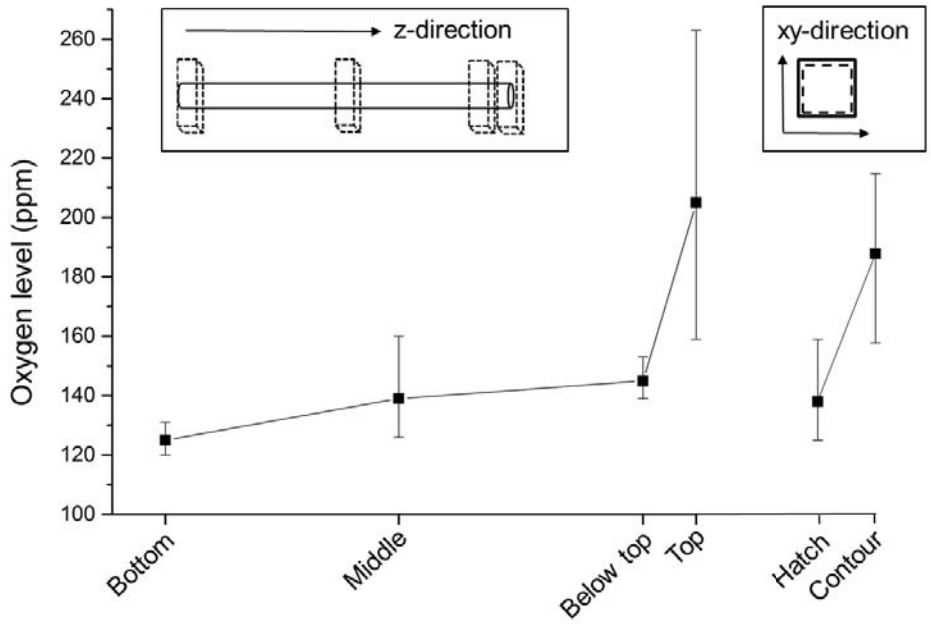

Fig. 28. Distribution of oxygen concentration in samples built from re-used powder.

Firstly, in the XY-plane, oxide from the re-used powder may accumulate in the molten metal as it moves with the electron beam, followed by deposition at the electron beam turning points, i.e. at the interface between the hatch and the contour region, as illustrated in Fig. 29 (a). Large, continuous oxide flakes in the contour region are most likely the reason for the higher amount of LOFDs in samples fabricated from re-used powder.

Furthermore, clusters of non-metallic inclusions (oxide and nitride) in the liquid metal float towards the melt pool surface. During layer re-melting, these inclusions may be transported further upwards, layer by layer along the build direction, as illustrated in Fig. 29 (b). Eventually, they may be entrapped as inclusions inside the metal matrix, as illustrated in Fig. 26. A certain amount, however, reaches the top surface, as seen in Fig. 18 (a).

In conclusion, transportation of oxide (and nitride) upwards and towards to the sample edges, as illustrated in Fig. 29 (c), has the effect that a certain amount of de-oxidation or refining takes place during the EBM process. This is also one of the reasons for the lower oxygen level in the solid samples compared to the powder from which it was built. The other being partial removal of nickel oxide/hydroxide layer from the initial powder by the electron beam in the vacuum, providing thermodynamically favourable conditions for oxide dissociation.

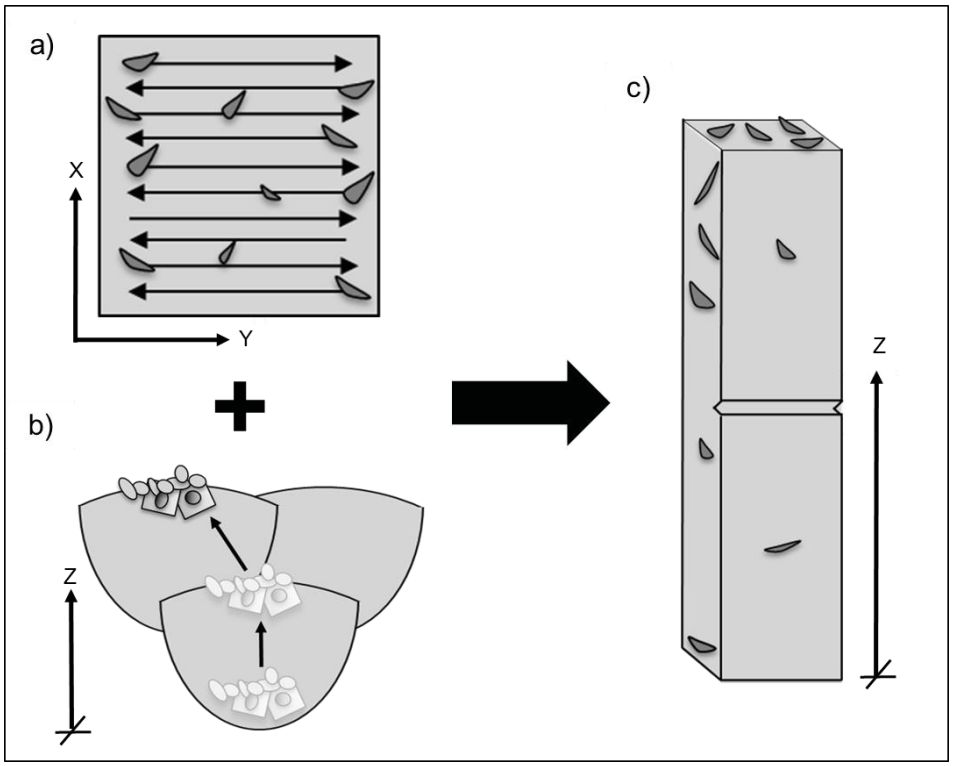

Fig. 29. Inclusion transfer mechanisms in the directions (a) perpendicular to and (b) along the build direction resulting in accumulation of oxide at the contour region as well as on the sample top surface (c).

7. CONCLUSIONS

The following conclusions can be drawn from this thesis study:

Alloy 718 powder undergoes significant oxidation while exposing the powder to the EBM process and the environment in the build chamber. Selective oxidation of Al under these conditions results in a transformation from the thin layer covering the virgin powder, to a coarse, heterogeneous layer consisting of thermodynamically stable Al-rich oxide particulates, together with a thin nickel oxide/hydroxide layer in between the particulates. This transformation starts already after the first build cycle and progresses with increasing number of re-use cycles. The increasing amount of oxide is confirmed by an increase in oxygen level with progressive re-use.

The oxide on the surface of the re-used powder acts as a source of oxygen for formation of oxide inclusions inside EBM fabricated samples, which therefore sees a corresponding increase with progressive powder re-use. The inclusion morphology depends on the conditions during melting and varies from finely dispersed oxide inclusions inside the lack of fusion defects (LOFDs) to large oxide flakes that have formed due to extensive agglomerates in the molten metal.

The hatch material in the EBM parts has a clearly lower oxygen level than the powder from which it is fabricated. This is promoted by oxide transportation upwards along the build direction as well as towards the contour region during the melting process, which lowers the amount of non-metallic phases in the hatch region.

Accumulation of oxide in the volume close the contour region result in an increasing of amount of LOFDs in this region with progressive powder re-use. Due to the presence of oxide inside many LOFDs in samples built from re-used powder, it remains after hot isostatic pressing.

Future work

A more thorough analysis of the surface phases as well as microstructure of the as-received and re-used powder conditions would provide a deeper understanding of the changes that occur during powder recycling. Similarly, in-depth analysis of oxide inclusions in the fabricated samples would provide further understanding regarding their origin and formation mechanisms.

Controlled laboratory experiments complemented by thermodynamic and kinetic simulations would be helpful to simulate powder oxidation at different conditions (temperature and oxygen level) in order to assess the possibility of minimizing powder degradation during EBM processing. Simulation can also be used to assess the conditions required to dissolve non-metallic phases (such as TiN) during powder production as well as EBM processing.

Non-metallic inclusions are known to have a negative influence on the mechanical properties of Ni-base and Ni-Fe-base superalloys and hence, the relevance of the findings in this work should be confirmed through mechanical testing. Especially, a critical effect on the fatigue performance has been reported, which should be evaluated from fatigue testing of test samples produced from virgin and re-used powder.

Acknowledgements

First I would off course like to thank my supervisor Prof. Eduard Hryha and my co-supervisor Prof. Lars Nyborg for giving me the opportunity to work with this exciting topic. I would also like to thank them both for their guidance, input and help throughout this work.

Recognitions to the Centre for Additive Manufacturing – Metal (CAM^2), supported by Vinnova, for enabling the framework within which this work has been performed. The author would like to acknowledge SIP LIGHTer and AoA Production at Chalmers for financial support.

Mikael Henriksson is greatly acknowledged, especially for being a very good friend, but also all the help with XPS and AES analyses, on which we have spent many days together. I would also like to thank my Master's thesis student Cosmina Luchian for the microscopy work and for our long discussions about defect formation.

Special appreciation is also expressed to Jonas Olsson at Production Technology Centre, Trollhättan, Sweden for his help with EBM processing and powder sampling. The same goes to Quintus technologies for HIPing the samples and to Höganäs AB for Charpy impact testing and bulk chemical analysis. Thanks to Niklas Israelsson and Simon Eichler at Arcam AB for input about the project results.

I also would like to acknowledge the research engineers Dr. Ruslan Shvab, Dr. Eric Tam, Dr. Yiming Yao, Dr. Yu Cao, Lic. Eng. Lars Hammar and Roger Sagdahl for their help regarding all practical work.

Thanks to all the colleagues at the Department of Industrial and Materials Science for making the time enjoyable. Special thanks to my roommate Kristina Karlsson, and also to Alex, Camille, Dmitri, Eric, Mikael, Johan, Maheswaran, Swathi, William, Masoud and Marie for all the discussion, ideas, and memorable stories created during our conferences.

Last but not least, I would like to thank my family and friends for reminding me of the world outside the office.

References

[1] P. N. Quested, D. M. Hayes, and K. C. Mills, "Factors affecting raft formation in electron beam buttons," *Mater. Sci. Eng. A*, vol. 173, no. 1–2, pp. 369–375, 1993.

[2] C. T. Sims, N. S. Stoloff, and W. C. Hagel, *Superalloys 2*, 2nd ed. Wiley, 1987.

[3] J. E. Matz and T. W. Eagar, "Carbide formation in alloy 718 during electron-beam solid freeform fabrication," *Metall. Mater. Trans. A*, vol. 33, no. 8, pp. 2559–2567, 2002.

[4] A. Leicht, "Aspects of building geometry and powder characteristics in powder bed fusion Department of Industrial and Materials Science," 2018.

[5] D. Deng, *Additively Manufactured Inconel 718 : Microstructures and Mechanical Properties*, no. 1798. 2018.

[6] R. Sprague, "GAS TURBINE," no. May, pp. 29–33, 2004.

[7] V. Sames, William James, "Additive manufacturing of Inconel 718 using electron beam melting: Processing, post-processing, & mechanical properties," no. May, p. 340, 2015.

[8] Z. Super, D. Stainless, A. A. G. F, B. Asme, S. Viii, D. Case, and S. Iii, "The Global Leader in Specialty Metals," vol. 718, no. Ams 5662, pp. 10–11, 2000.

[9] I. Gibson, D. Rosen, and B. Stucker, *Additive Manufacturing Technologies*, 2nd ed. 2015.

[10] W. J. Sames, K. A. Unocic, R. R. Dehoff, T. Lolla, and S. S. Babu, "Thermal effects on microstructural heterogeneity of Inconel 718 materials fabricated by electron beam melting," *J. Mater. Res.*, vol. 29, no. 17, pp. 1920–1930, 2014.

[11] E. Chauvet, P. Kontis, E. A. Jägle, B. Gault, D. Raabe, J.-J. Blandin, R. Dendievel, B. Vayre, S. Abed, G. Martin, and C. Tassin, "Hot cracking mechanism affecting a non-weldable Ni-based superalloy produced by Selective Electron Beam Melting," *Acta Mater.*, vol. 142, no. 17, pp. 82–94, 2017.

[12] A. T. Polonsky, M. P. Echlin, W. C. Lenthe, R. R. Dehoff, M. M. Kirka, and T. M. Pollock, "Defects and 3D structural inhomogeneity in electron beam additively manufactured Inconel 718," *Mater. Charact.*, no. January, 2018.

[13] M. Esperon-miguez, "The present and future of additive manufacturing in the aerospace sector : A review of important aspects," no. October, 2015.

[14] H. E. Helmer, C. Körner, and R. F. Singer, "Additive manufacturing of nickel-based superalloy Inconel 718 by selective electron beam melting: Processing window and microstructure," *J. Mater. Res.*, vol. 29, no. 17, pp. 1987–1996, 2014.

[15] K. Wegener, F. Kuster, S. Weikert, L. Weiss, and J. Stirnimann, "Success Story Cutting," vol. 46, pp. 512–524, 2016.

[16] S. Olovsjö, "Influence of microstructure in machining of nickel and nickel-iron based superalloys," Chalmers university of technology, 2011.

[17] Maher, "Alloy 718 Data Sheet Quick Facts Alloy 718 Data Sheet Industry Specifications Melting Practices Machinability," pp. 1–5.

[18] D. Zhu, X. Zhang, and H. Ding, "Tool wear characteristics in machining of nickel-based superalloys," *Int. J. Mach. Tools Manuf.*, vol. 64, pp. 60–77, 2013.

[19] D. T. Fakultät and H. E. Helmer, "Additive Fertigung durch Selektives Elektronenstrahlschmelzen der Nickelbasis Superlegierung IN718 : Prozessfenster , Mikrostruktur und mechanische Eigenschaften."

[20] European powder metallurgy association, *Introduction to additive manufacturing technology - a guide for designers and engineers*, 2nd ed. 2017.

[21] Höganäs AB, "https://www.hoganas.com/en/powder-technologies/additive-manufacturing/products/nickel-based/," 2018. .

[22] M. I. Moulding, J. Kroeger, and R. Ap, "Raymor AP & C : Leading the way with plasma atomised Ti spherical powders for MIM," vol. 5, no. 4, pp. 55–57, 2011.

[23] K. Dietrich, P. Forêt, D. Bauer, and G. Witt, "How Porosity Is Affected By Different Residual Oxygen Concentrations In The Building Chamber During Laser Powder Bed

Fusion (L-PBF)," *EuroPM2018*, 2018.
[24] S. Biamino, A. Penna, U. Ackelid, S. Sabbadini, O. Tassa, P. Fino, M. Pavese, P. Gennaro, and C. Badini, "Electron beam melting of Ti-48Al-2Cr-2Nb alloy: Microstructure and mechanical properties investigation," *Intermetallics*, vol. 19, no. 6, pp. 776–781, 2011.
[25] P. Nandwana, W. H. Peter, R. R. Dehoff, L. E. Lowe, M. M. Kirka, F. Medina, and S. S. Babu, "Recyclability Study on Inconel 718 and Ti-6Al-4V Powders for Use in Electron Beam Melting," *Metall. Mater. Trans. B Process Metall. Mater. Process. Sci.*, vol. 47 B, no. 1, pp. 754–762, 2016.
[26] A. Leicht, R. Shvab, E. Hryha, and L. Nyborg, "Characterization of virgin and recycled 316L powder used in additive manufacturing."
[27] X. Wang, X. Gong, and K. Chou, "Review on Powder-Bed Laser Additive Manufacturing of Inconel 718 Parts," *ASME 2015 Int. Manuf. Sci. Eng. Conf. Am. Soc. Mech. Eng.*, no. JUNE 2015, pp. 1–9, 2015.
[28] M. Renderos, A. Torregaray, M. E. Gutierrez-Orrantia, A. Lamikiz, N. Saintier, and F. Girot, "Microstructure characterization of recycled IN718 powder and resulting laser clad material," *Mater. Charact.*, vol. 134, no. September, pp. 103–113, 2017.
[29] A. Strondl, O. Lyckfeldt, H. Brodin, and U. Ackelid, "Characterization and Control of Powder Properties for Additive Manufacturing," *Jom*, vol. 67, no. 3, pp. 549–554, 2015.
[30] V. Petrovic and R. Niñerola, "Powder recyclability in electron beam melting for aeronautical use," *Aircr. Eng. Aerosp. Technol.*, vol. 87, no. 2, pp. 147–155, 2015.
[31] S. B. Park, B. Road, and U. Kingdom, "Investigating the effects of multiple re-use of Ti6Al4V powder in additive manufacturing," *Renishaw*, pp. 1–10, 2016.
[32] R. Samant, A. Engineer, B. Lewis, and P. Technician, "Metal Powder Recycling and Reconditioning in Additive Manufacturing."
[33] H. P. Tang, M. Qian, N. Liu, X. Z. Zhang, G. Y. Yang, and J. Wang, "Effect of Powder Reuse Times on Additive Manufacturing of Ti-6Al-4V by Selective Electron Beam Melting," *Jom*, vol. 67, no. 3, pp. 555–563, 2015.
[34] E. Hryha, E. Dudrova, and L. Nyborg, "On-line control of processing atmospheres for proper sintering of oxidation-sensitive PM steels," *J. Mater. Process. Technol.*, vol. 212, no. 4, pp. 977–987, 2012.
[35] S. Das, "Physical Aspects of Process Control in Selective Laser Sintering of Metals," *Adv. Eng. Mater.*, vol. 5, no. 10, pp. 701–711, 2003.
[36] C. Gierl-Mayer, R. de Oro Calderon, and H. Danninger, "The Role of Oxygen Transfer in Sintering of Low Alloy Steel Powder Compacts: A Review of the 'Internal Getter' Effect," *Jom*, vol. 68, no. 3, pp. 920–927, 2016.
[37] Q. Jia and D. Gu, "Selective laser melting additive manufactured Inconel 718 superalloy parts: High-temperature oxidation property and its mechanisms," *Opt. Laser Technol.*, vol. 62, pp. 161–171, 2014.
[38] K. Sung Hwan, K. Chaewon, and O. S. Gokul, "Corrosion and Carburization Behaviour of Ni-Cr-Mo-Nb Superalloys in a High Temperature Supercritical-CO2 Environment," in *Proceedings of the 9th International Symposium on Superalloy 718 and derivatives*, 2018, pp. 179–192.
[39] R. Molins and E. Andrieu, "Analytical TEM study of the oxidation of nickel based superalloys To cite this version : HAL Id : jpa-00252390 Analytical TEM study of the oxidation of nickel based superalloys," 1993.
[40] V. N. Shukla, R. Jayaganthan, and V. K. Tewari, "Oxidation and Hot Corrosion Behaviour of Ni-based Superalloy Inconel 718 in Na 2 So 4 -75 % V 2 O 5 Environment at Elevated Temperature," vol. 3, no. 1, pp. 20–24, 2013.
[41] E. Sadeghi, P. Karimi, P. Zhang, R. Peng, J. Andersson, L. Pejryd, and S. V. Joshi, "Isothermal Oxidation Behavior of EBM-Additive Manufactured Alloy 718," in *Proceedings of the 9th International Symposium on Superalloy 718 and derivatives*, 2018, pp. 219–239.
[42] V. Garat, J. Deleume, J. Cloué, and E. Andrieu, "HIGH TEMPERATURE

INTERGRANULAR OXIDATION OF ALLOY 718," pp. 559–569, 2005.
[43] I. Olefjord and L. Nyborg, "Surface Analysis of Gas Atomized Ferritic Steel Powder," *Powder Metall.*, vol. 28, no. 4, pp. 237–243, 1985.
[44] L. Nyborg and I. Olefjord, "SURFACE ANALYSIS OF REP-ATOMIZED MARTENSITIC STEEL POWDER," *Powder Metall. Int.*, vol. 20, no. 2, pp. 11–16, 1988.
[45] M. Saunders, "Oxygen algebra - does yours add up ?," no. November 2016, pp. 1–8, 2017.
[46] L. C. Ardila, F. Garciandia, J. B. González-Díaz, P. Álvarez, A. Echeverria, M. M. Petite, R. Deffley, and J. Ochoa, "Effect of IN718 recycled powder reuse on properties of parts manufactured by means of Selective Laser Melting," *Phys. Procedia*, vol. 56, no. C, pp. 99–107, 2014.
[47] M. Galati and L. Iuliano, "A literature review of powder-based electron beam melting focusing on numerical simulations," *Addit. Manuf.*, vol. 19, pp. 1–20, 2018.
[48] Y. N. Zhang, X. Cao, P. Wanjara, and M. Medraj, "Oxide films in laser additive manufactured Inconel 718," *Acta Mater.*, vol. 61, no. 17, pp. 6562–6576, 2013.
[49] L. Rickenbacher, T. Etter, S. Hövel, and K. Wegener, "High temperature material properties of IN738LC processed by selective laser melting (SLM) technology," *Rapid Prototyp. J.*, vol. 19, no. 4, pp. 282–290, 2013.
[50] M. M. Attallah, R. Jennings, X. Wang, and L. N. Carter, "Additive manufacturing of Ni-based superalloys: The outstanding issues," *MRS Bull.*, vol. 41, no. 10, pp. 758–764, 2016.
[51] S. Tammas-Williams, P. J. Withers, I. Todd, and P. B. Prangnell, "Porosity regrowth during heat treatment of hot isostatically pressed additively manufactured titanium components," *Scr. Mater.*, vol. 122, pp. 72–76, 2016.
[52] M. H. Manjili and M. Halali, "Removal of Non-metallic Inclusions from Nickel Base Superalloys by Electromagnetic Levitation Melting in a Slag," *Metall. Mater. Trans. B Process Metall. Mater. Process. Sci.*, vol. 49, no. 1, pp. 61–68, 2018.
[53] Y. Haruna, "Removal of inclusions from cast superalloy revert," University of British Columbia, 1994.
[54] A. Mitchell, "Recent Developments in Superalloy Melting Technology," *Key Eng. Mater.*, vol. 77–78, pp. 177–186, 1992.
[55] S. L. Cockcroft, T. Degawa, a Mitchell, D. W. Tripp, and a Schmalz, "Inclusion Precipitation in Superalloys," *Superalloys 1992*, pp. 577–586, 1992.
[56] A. Mitchell, A. J. Schmalz, C. Schvezov, and S. L. Cockcroft, "The Precipitation of Primary Carbides in Alloy 718," *Superalloys 718, 625, 706 Var. Deriv.*, pp. 65–78, 1994.
[57] a. Mitchell, "The Present Status of Melting Technology for Alloy 718," *Superalloys 718 Metall. Appl.*, pp. 1–15, 1989.
[58] A. Mitchell, "Progress in Understanding Clean Metal Production for IN718," *Superalloys 718, 625 Var. Deriv.*, pp. 109–124, 1994.
[59] D. Krewerth, T. Lippmann, A. Weidner, and H. Biermann, "Influence of non-metallic inclusions on fatigue life in the very high cycle fatigue regime," *Int. J. Fatigue*, vol. 84, pp. 40–52, 2016.
[60] M. L. Harris, "A study on non-metallic inclusions in foundry steel process," *ProQuest Diss. Theses*, p. 94, 2016.
[61] M.-A. Van Ende, *Formation and Morphology of non-Metallic Inclusions in Aluminium Killed Steels*. 2010.
[62] A. Balachandramurthi, J. Moverare, N. Dixit, and R. Pederson, "Influence of defects and as-built surface roughness on fatigue properties of additively manufactured Alloy 718," *Mater. Sci. Eng. A*, vol. 735, pp. 463–474, 2018.
[63] Y. Sun, R. Hebert, and M. Aindow, "Non-Metallic Inclusions in 17-4PH Stainless Steel Parts Produced by Selective Laser Melting," *Mater. Des.*, vol. 140, pp. 153–162, 2018.
[64] X. Xu, J. Ding, S. Ganguly, C. Diao, and S. Williams, "Oxide accumulation effects on wire + arc layer-by-layer additive manufacture process," *J. Mater. Process. Technol.*, vol. 252, no.

July 2017, pp. 739–750, 2018.
[65] L. Thijs, J. Van Humbeeck, K. Kempen, E. Yasa, J. Kruth, and M. Rombouts, "Investigation on the inclusions in maraging steel produced by Selective Laser Melting," *Innov. Dev. Virtual Phys. Prototyp.*, pp. 297–304, 2011.
[66] J. Campbell and M. Tiryakiog, "Bifilm Defects in Ni-Based Alloy Castings," 2012.
[67] A. Cooke and J. Slotwinski, "Properties of Metal Powders for Additive Manufacturing: A Review of the State of the Art of Metal Powder Property Testing," 2012.